High mortality of *Acinetobacter baumannii* infection is attributed to macrophage-mediated induction of cytokine storm but preventable by naproxen

Han Wang,[a,b,d] Qi Xu,[b,d] Heng Heng,[a,b] Wenxing Zhao,[b] Hongyuhang Ni,[a,b] Kaichao Chen,[b] Bill Kwan Wai Chan,[b] Yang Tang,[a,b] Miaomiao Xie,[b] Mingxiu Peng,[c] Edward Wai Chi Chan,[b] Guan Yang,[a,*] and Sheng Chen[b,c,**]

[a]Department of Infectious Diseases and Public Health, Jockey Club College of Veterinary Medicine and Life Sciences, City University of Hong Kong, Kowloon, Hong Kong SAR, China
[b]State Key Lab of Chemical Biology and Drug Discovery and the Department of Food Science and Nutrition, The Hong Kong Polytechnic University, Kowloon, Hong Kong SAR, China
[c]Shenzhen Key Lab for Food Biological Safety Control, The Hong Kong Polytechnic University Shenzhen Research Institute, Shenzhen, 518057, China

eBioMedicine
2024;108: 105340
Published Online xxx
https://doi.org/10.1016/j.ebiom.2024.105340

Summary

Background The continuous emergence of multidrug-resistant (MDR) *Acinetobacter baumannii* (*Ab*) strains poses further challenges in its control and clinical management. It is necessary to decipher the mechanisms underlying the high mortality of *Ab* infections to explore unconventional strategies for controlling outbreaks of drug-resistant infections.

Methods The immune responses of *Ab* sepsis infection were investigated using flow cytometry, RNA-seq, qRT-PCR, and ELISA and scRNA-seq. The detailed pathways mediating *Ab* immune responses were also depicted and a specific therapy was developed based on the understanding of the mechanisms underlying *Ab*-induced cytokine storms.

Findings The results highlighted the critical role of alveolar and interstitial macrophages as targets of *Ab* during the infection process. These cells were found to undergo polarization towards the M1 phenotype, triggering a cytokine storm that eventually caused the death of the host. The polarization and excessive inflammatory response mediated by macrophages were mainly regulated by the TLR2/Myd88/NF-κB signaling pathway. Suppression of *Ab*-triggered inflammatory responses and M1 polarization by the drug naproxen (NPXS) was shown to confer full protection of mice from lethal infections.

Interpretation The findings in this work depict the major mechanisms underlying the high mortality rate of *Ab* infections and highlight the clinical potential application of anti-inflammatory drugs or immunosuppressants in reducing the mortality of such infections, including those caused by MDR strains.

Funding Funding sources are described in the acknowledgments section.

Keywords: *Acinetobacter baumannii*; Sepsis; Macrophage polarization; Cytokine storm; Toll-like receptor 2 (TLR2); Naproxen

Introduction

Acinetobacter baumannii (*Ab*) is an opportunistic bacterial pathogen that primarily infects immunocompromised individuals. Hospital infections caused by *Ab* have become a global health concern in recent years due to the emergence of multidrug-resistant (MDR) strains.[1,2] This pathogen can cause infections at various body sites, such as skin, soft tissue, and the urinary tract. More serious infections including ventilator-related pneumonia and sepsis are associated with an

*Corresponding author. Department of Infectious Diseases and Public Health, City University of Hong Kong, Kowloon, Hong Kong SAR, 999077, China.
**Corresponding author. State Key Lab of Chemical Biology and Drug Discovery and the Department of Food Science and Nutrition, The Hong Kong Polytechnic University, Hung Hom, Kowloon, Hong Kong SAR, China.
E-mail addresses: gyang25@cityu.edu.hk (G. Yang), sheng.chen@polyu.edu.hk (S. Chen).
[d]These authors contributed to the work equally and should be regarded as co-first authors.

Research in context

Evidence before this study

We searched PubMed for articles published in English containing the terms "*Acinetobacter baumannii*" and "sepsis" from the inception of the database to February 14th, 2024. A total of 1149 articles were identified on this topic, suggesting that *Ab*-induced sepsis has been recognized as a significant global public health concern. However, the mechanisms underlying the mortality caused by *Ab* infection remain unexplored. In addition, there is a lack of studies examining the association between *Ab* infection and macrophage polarization-mediated cytokine storm.

Added value of this study

In this study, we discovered that *Ab* cannot be effectively cleared by the immune system, resulting in continuous stimulation of alveolar and interstitial macrophages and their polarization towards the M1 phenotype. Mechanistically, *Ab*-induced macrophage polarization was triggered by the activation of the TLR2/MyD88/NF-κB signaling pathway and was correlated with the occurrence of a cytokine storm, leading to tissue damage and host death. Importantly, we demonstrated that NPXS could suppress M1 polarization and a wide range of host inflammatory responses, thereby reducing the mortality in the mouse model of *Ab* infection.

Implications of all the available evidence

This study provides evidence that macrophage polarization-mediated cytokine storm is a significant contributor to *Ab*-triggered sepsis, shedding light on the underlying mechanism behind the high mortality rate associated with *Ab* infections. Furthermore, the effectiveness of NPXS in controlling *Ab* infection in mice by suppressing the acute cytokine storm offers innovative approaches for treating MDR *Ab* strains infection and opens the possibility of introducing NPXS into clinical applications through further clinical trials.

unacceptably high mortality rate.[3,4] The difficulty in treating clinical *Ab* infections has further increased due to the continuous evolution of drug-resistance phenotypes particularly the high rate of resistance to carbapenems.[5,6] A lack of active and broad-spectrum antimicrobials has prompted the development of novel therapies to control these infections.

For the effective containment and treatment of MDR *Ab*, it is critical to thoroughly understand the immune response and the molecular mechanisms triggered by *Ab* infection in the host. Utilizing mouse models, numerous studies have explored the host immune response to *Ab* infection, revealing the local recruitment of macrophages and neutrophils, along with the production of chemokines and proinflammatory cytokines.[7–9] Macrophages play a pivotal role in maintaining the inflammatory microenvironment during *Ab* infection. In the early stages of bacterial infection, macrophages are intentionally polarized toward the M1 phenotype, releasing substantial proinflammatory cytokines.[9] However, uncontrolled macrophage-mediated inflammatory responses may lead to cytokine storm, a life-threatening systemic inflammatory syndrome caused by excessive elevation of cytokine levels and hyperactivation of immune cells.[10]

Furthermore, current data show that *Ab* infection-induced sepsis is attributed to dysregulation of the innate immune system, which is mediated by pattern recognition receptors (PRRs). Toll-like receptors (TLRs), a membrane-bound PRR, are pivotal to initiating the immune response but are also responsible for regulating the degree of inflammatory response by recognizing specific pathogen-associated molecular patterns (PAMPs) of *Ab*.[11,12] TLR2 and TLR4 play critical roles in eliciting innate immune responses against *Ab* infection.[13,14] Lipopolysaccharide (LPS) could be recognized by TLR4 in the host and trigger the activation of mitogen-activated protein kinase (MARK) and nuclear factor kappa-B (NF-κB). This activation facilitated IL-6, IL-12, and TNF-α production by dendritic cells and macrophages.[15] Additionally, TLR2 also can recognize various microbial structures, including porins and lipoproteins expressed by *Ab*.[16] In a mouse model of *Ab* infection, TLR2 is vital in inducing IL-8 production from airway epithelial cells.[17] A comprehensive investigation of the *Ab*-induced immune response *in vivo* can help identify potential targets for the development of novel approaches for the treatment of *Ab* infections.

In this study, we found that alveolar macrophages (AMs) and interstitial macrophages (IMs) are the key components of the host immune system that regulate the changes in *Ab*-induced inflammatory microenvironment. These macrophages could undergo polarization toward the M1 phenotype and cause the onset of cytokine storm, resulting in death of the host. Furthermore, we found that the M1 polarization event triggered by *Ab* was mainly mediated by the TLR2/MyD88/NF-κB signaling pathway and that this even would result in cytokine over-production. Importantly, we showed that the drug naproxen (NPXS) could effectively suppress excessive inflammatory response in infected mice, thereby protecting the infected mice from death. These findings suggest that the use of immunosuppressive drugs represents a promising therapeutic strategy for the management of acute *Ab* infection.

Methods

Cells

RAW 264.7 murine macrophages were purchased from the American Type Culture Collection (ATCC) and

grown in Dulbecco's modified Eagle medium (DMEM) medium supplemented with 10% heat-inactivated fetal bovine serum (FBS).

Bacterial strains and culture condition

Ab strain ATCC 17978 was purchased from the American Type Culture Collection (VA, USA), and was incubated in LB broth and agar plates at 37 °C unless stated otherwise. When required, 50 μg/mL of cloxacillin was added for selection purposes.

Reagents and resources

Reagents and resources are summarized in Supplemental Table S1.

Mice used in this study

C57BL/6 and *Tlr2*$^{-/-}$ mice (5–7 weeks old) were employed for animal experiments. Both male and female mice, 6–8 weeks old age- and sex-matched, were used in this study. C57BL/6 mice (RRID: MGI:2159769) were provided by the Laboratory Animal Research Unit of the City University. *Tlr2*$^{-/-}$ mice (RRID: IMSR_NM-KO-18026) were purchased from Shanghai Model Organisms Center (Shanghai, China), bred in-house at the Hong Kong Polytechnic University Shenzhen Research Institute, and previously used as a model for studying inflammatory responses and related diseases.[18–21] Upon weaning, C57BL/6 and *Tlr2*$^{-/-}$ mice were randomized into standard-density cages and housed in sterile isolators at 21 °C under 12:12 dark/light cycles, with access to enough water and food. The genotype of KO mice was identified by PCR with primers listed in Supplementary Table S2.

Ethics

The Hong Kong Polytechnic University Animal Ethics Committee and the City University of Hong Kong Animal Research Ethics Sub-Committee approved this study. All animal experiments were approved by the Laboratory Animal Research Unit of the City University of Hong Kong (approval number AN-STA-00000194) and Hong Kong Polytechnic University Shenzhen Research Institute (approval number 23-24/821-FSN-R-TRS).

Mouse sepsis infection model

The mouse infection model was employed to detect the immune response induced by *Ab in vivo*. Power calculations were not performed, and sample sizes were determined from prior preclinical studies. Mice were randomly divided into two groups (5 animals per group in a cage): non-infected group and *Ab*-infected group by intraperitoneal injection of 7.5×10^7 CFU of ATCC 17978. The body weight of all mice was recorded before infection and at 12 h post-infection (hpi). Survival of the test animals was determined by recording the mortality rate throughout the entire 120 h experimental period. Blinding procedures were not implemented. At 12 hpi, the mice were sacrificed, and the organs were collected and homogenized for bacterial load measurement and analysis by flow cytometry, RNA-seq, scRNA-seq, and qRT-PCR assay. The serum of the mice was collected for ELISA detection. Animal experiments were conducted at least twice to assess the consistency of the data.

Collection of spleen and lung single cell

To collect lung cells, the entire lung sample was minced into a homogenous paste by scalpel and digested in HBSS containing 1 × HEPES and 0.4 mg/mL Collagenase I (Thermo Fisher Scientific, Cat# 17100017) for 1 h at 37 °C. The digested tissues were mashed through a 70 μm strainer to obtain lung cell suspension. Cells from spleens were pushed through a 70 μm strainer and allowed to fall into RPMI 1640 medium with 5% FBS. ACK lysing buffer (Thermo Fisher Scientific, Cat# A1049201) was used to lyse the erythrocyte.[22]

Determination of bacteria burden *in vivo*

To measure the total bacterial load in different organs, including the lung, spleen, liver, kidney homogenate, and blood samples, serial dilutions were prepared and plated onto agar plates containing 50 μg/mL cloxacillin. To further assess the number of intracellular bacteria *in vivo*, the lungs and spleens single cell suspension was washed with PBS twice and suspended in RPMI 1640 medium containing 5% FBS with 300 μg/mL gentamicin to eliminate the extracellular bacteria by incubation at 37 °C for 2 h. The cells were then lysed with 0.2% Triton X-100 and the cell lysates were also spread onto the agar plates to count the number of phagocyted bacteria.

Flow cytometric analysis

Single lung and spleen cells isolated from the test mice were incubated with different combinations of fluorochrome-conjugated antibodies against mice: CD45 (Cat# 103106), CD11b (Cat# 101235), Ly6G (Cat# 127615), F4/80 (Cat# 123113), CD206(Cat# 141703), CD86 (Cat# 105029), CD3 (Cat# 100235), CD19 (Cat# 115529), CD4 (Cat# 100437), CD8 (Cat# 100751), NK1.1 (Cat# 156513), TLR2 (Cat# 153006); appropriate isotype controls were acquired from Biolegend. Ghost dye ™ violet 510 (Tonbo Biosciences, Cat#13-0870-T100) or Propidium iodide (Sigma–Aldrich, Cat#P4170-1G) was used to exclude dead cells. Flow cytometric analyses were carried out by using a FACSCelesta™ flow cytometer (BD Biosciences, CA, USA); data analysis was conducted by FlowJo software (Version 10.8.1, Treestar, CA, USA).

RNA extraction and real-time quantitative PCR assay

Total RNA was extracted from the homogenized lung samples or RAW 264.7 cells (ATCC, CA, USA) upon *Ab* infection, utilizing the TRIzol™ method (Thermo Fisher

Scientific, Cat#15596026). Turbo DNA-free™ Kit (Invitrogen, Cat#AM1907) was employed for removal of DNA contaminants. 1 μg purified mRNA was reverse transcribed into cDNA using SuperScript™ III First-Strand Synthesis SuperMix Kit (Invitrogen, Cat#18080400), with a 1:10 dilution for subsequent qRT-PCR analysis. The qRT-PCR was then performed on an ABI QuantStudio 7 Flex Real-Time PCR System (Applied Biosystems, CA, USA) by the PowerUP SYBR Green master mix (Applied Biosystems, Cat#A25724). The primers used are shown in Supplementary Table S2. The target gene transcription levels were quantified by the comparative Ct method and normalized to the expression level of glyceraldehyde-3-phosphate dehydrogenase (GADPH).

RNA sequencing

Total RNA extracted from lung samples was sequenced by Novogene Technology (Hong Kong SAR, China). Bioanalyzer 2100 system (Agilent Technologies, CA, USA) was used to measure RNA integrity; the NEBNextUltra RNA Library Prep Kit (NEB, Cat#E7770) was employed to construct the cDNA libraries for Illumina sequencing. The index-coded samples clustering was carried out on a cBot Cluster Generation System by the TruSeq PE Cluster Kit v3-cBot-HS (Illumia, Cat#PE-401-3001). The libraries were sequenced on the Illumina Novaseq platform with paired-end 150 bp reads. HISAT2 was used for sequencing reads alignment.[23] Fragments per gene were counted based on exon regions with FeatureCounts v.1.6.2.[24] Differential mRNA level analysis was carried on by the DESeq2 R package.[25] Unigenes with P.adjust <0.05 and |Log2Fold Change| > 1 could be described as differentially expressed genes. Gene Enrichment Analysis was conducted for gene ontology enrichment analysis. The up/down-regulated DEGs were visualized by volcano plots.

Serum collection

Blood was collected from the test mice by orbital bleeding and clotted at RT for 1 h. Blood was subsequently subjected to centrifugation at 10,000 g for 25 min at 4 °C. Serum was divided into tubes and stored immediately at –80 °C until cytokine analysis.

Cytokine analysis

The enzyme-linked immunosorbent assay (ELISA) was used to perform cytokine analysis in mouse serum and cell supernatants. Mouse serum was extracted as described above. Pre-treated macrophage cell supernatants were harvested and centrifuged to remove impurities. The levels of IL-1β, IL-6, and TNF-α were measured by using the IL-1β, IL-6, and TNF-α Mouse Uncoated ELISA Kit (Thermo Fisher Scientific, Cat#88-7013-86, Cat#88-7064-88, Cat#88-7324-88) according to the manufacturer's protocols, respectively.

Single-cell RNA sequencing and data processing

The single cell suspension extracted from mouse lung samples was sent to BGI Genomics (Hong Kong SAR, China) for 10 × genomics single-cell sequencing. Briefly, the 10 × Genomics® Chromium™ Next GEM Single Cell 3′ Library Construction Kit v3.1 (10 × Genomics, Cat# rxns PN-1000121) were employed to build premade libraries. After quality analysis of premade libraries, they were converted to DNBs (DNA Nanospheres) for sequencing using BGI's proprietary DNBseq™ NGS technology. De-multiplexing, barcode processing, and single-cell 5′ Unique Molecular Identifier (UMI) enumeration were performed by using the Cell Ranger Software Suite (v.3.1.0). The valid cells were filtered based on gene number, UMI count, and gene percentage of mitochondrial.

Dimensionality reduction and clustering

The filtered gene barcode matrix for all samples was integrated and normalized by Seurat v.4.3 with default parameters.[26] Highly variable genes were verified by the "vst" method within the Seurat FindVariableFeatures function. The variables "percent.mito" and "nCount_RNA" were regressed in the scaling step. PCA was conducted with highly variable genes. To visualize the cells, UMAP was carried out on the top – principal components. Also, the resolution was set to 0.2 to perform graph-based clustering analysis on PCA-reduced data. All clusters were subjected to differential gene expression analysis by FindAllMarkers to verify the marker genes concerned. Marker genes of each cluster were selected according to a normalized RNA expression value (RNA expression values > 0.25 log-fold higher than the mean expression value and detectable expression in >25% of all cells) to annotate fine clusters. AMs and IMs were also re-integrated and re-clustered in the same manner.

Cell–cell communication analysis

The CellChat (v1.6.1) package is utilized to infer, analyze, and visualize cell–cell communication between various immune cells, using the CellChat database (https://github.com/sqjin/CellChat) as a reference. For cellular interaction analysis, the expression levels related to the total number of reads were calculated and mapped to the same set of coding genes across all transcriptomes. Expression values were averaged in each cell sample or single-cell cluster. Differential analysis of intercellular communication between infected and non-infected groups was performed by calculating and comparing the information flow of each signaling pathway, defined as all communication probabilities between all pairs of cell populations in the inferred network.

Pseudotime trajectory analysis

Trajectory analysis was conducted by Monocle version 3[27] to study the relationship between trajectories and macrophage subpopulations, after specifying the

corresponding cell as the root node. We utilized the 'plot_cells' function to visualize the pseudotime trajectory and ordered all cells, as well as cells from healthy or *Ab*-infected donors, onto the trajectory.

Differentially gene expression and KEGG pathway enrichment analysis

The analysis of differential gene expression was conducted by utilizing the FindAllMarkers in Seurat. The one-tailed Wilcoxon rank sum test was carried out, and *p*-values were adjusted for multiple testing by Bonferroni correction. Differentially expressed genes (DEGs) with adjusted P value < 0.01 were used for KEGG pathway enrichment analysis by the R package clusterProfiler.[28]

Mouse Ly6G$^+$ neutrophils isolation

Lung single-cell suspensions were sorted on a MojoSort™ magnet through the use of the MojoSort™ Mouse Ly-6G Selection Kit (Biolegend, Cat#480124) to select Ly6G$^+$ neutrophils. Briefly, Ly6G$^+$ cells were labeled by mixing the sample with the biotin antibody cocktail, followed by the addition of magnetic Streptavidin Nanobeads. These magnetically labeled cells were maintained by the magnetic separator. The purity of cells enriched from single-cell populations was consistently >90%, which fulfilled the requirement by flow cytometry.

Inhibitor treatment in RAW 264.7

RAW 264.7 cells were pre-treated for 1 h with the culture medium, C29 (100 μM),[29] TJ-M2010-5 (20 μM),[30] JSH-23 (30 μM),[28] and NPXS (30 μM, 60 μM) (MCE, Cat#HY-100461, Cat#HY-139397, Cat#HY-13982, and Cat#HY-15030A) respectively, and then stimulated with *Ab* (MOI = 5) for 6 h in the presence of the culture medium, C29, TJ-M2010-5, JSH-23 or NPXS. For cytokine measurement, cell supernatant was collected and centrifuged at 6500 g for 5 min to remove remained bacteria. For flow cytometry analysis, RAW 264.7 cells were incubated with fluorescently labeled antibodies against mouse F4/80, CD206, and CD86 for flow cytometric analysis, following washes three times with PBS and resuspension in PBS containing 2.5% FBS. For immunoblot analysis, cells were washed once with PBS and then lysed in RIPA buffer (containing protease and phosphatase inhibitors).

Immunoblot analysis

Protein concentration was measured by conducting BCA protein assay (Thermo Fisher Scientific, Cat#23227). 15 μg cell lysates were loaded on 12% SDS-PAGE gel and subsequently electroblotted to polyvinylidene difluoride membranes (Millipore, MA, USA) by a trans-blot turbo transfer system (Bio-rad, CA, USA). Non-specific binding was blocked by 5% skim milk in TBST, and then membranes were incubated overnight at 4 °C with primary antibodies against: IKKα (Cell Signaling Technology [CST], Cat#61294), IKKβ (CST, Cat#8943), phosphor-IKKα/β-Ser176/180 (CST, Cat#2697), IκBα (CST, Cat#4812), phospho-IκBα-Ser32 (CST, Cat#2859), NF-κB p65 (CST, Cat#8242), phospho-NF-κB p65-Ser536 (CST, Cat#3033), and beta-actin(Bioss, Cat#bs-0061R). Membranes were washed with TBST and incubated with HRP-linked secondary antibodies (CST, Cat#7074). Immunoreactive bands were visualized by Western HRP Substrate (Advansta, Cat#K-12043-D10).

OmpA gene knockout by CRISPR-Cas9-based genome editing platform

A two-plasmids genome-editing system, pSGAb-pCasAb, which combined the CRISPR-Cas9 genome cleavage system and the RecAb recombination system, was used in this study to perform efficient gene deletion in strain ATCC 17978.[31,32] A specific 20-bp spacer sequence (sgRNA) upstream of a PAM site of *OmpA* was selected by the sgRNAcas9 software[33] and cloned into the pSGAb-spe plasmid (Addgene, Cat#122000). Competent cells of ATCC 17978 were prepared by subculturing an overnight culture in LB broth, followed by culture at 37 °C with shaking until the OD_{600} value reached 0.4–0.7. The fresh exponentially growing culture was then washed with ddH_2O and then 10% glycerol which had been chilled to 4 °C. The pCasAb-apr plasmid (Addgene, Cat#121998) was then transformed into the competent cells of ATCC 17978 by electroporation. Upon being allowed to recover in LB broth for 1 h, the mixture was spread onto selective LB agar plates with 100 μg/mL apramycin. Transformants harboring the pCasAb-apr plasmid were selected and enriched by incubating at 37 °C until OD600 reached 0.1–0.15, followed by addition of IPTG to achieve 1 mM final concentration to induce expression of the Cas9 nuclease and the RecAb recombination system; the mixture was then further incubated for 2 h, followed by washing with ddH_2O and then 10% glycerol at 4 °C. In the next step, the ssDNA (ATCC 17978 genome repair template by homologous recombination) and sgRNA-introduced pSGAb-spe plasmids were simultaneously transformed into ATCC 17978 carrying the pCasAb-apr plasmid by electroporation. For recovery and genome editing, the culture was incubated for another 1.5 h before being spread onto LB agar plates with 100 μg/mL apramycin and 50 μg/mL spectinomycin. After incubation overnight, the colonies were collected and subjected to confirmation of whether the *ompA* gene had been deleted by PCR and nucleotide sequencing. The PCR validation results of ATCC 17978 and Δ*OmpA* are shown in Supplementary Figure S11, and the primers and ssDNA used in this study are listed in Supplementary Table S2.

Bacterial adherence, invasion, and survival in RAW 264.7 cell cultures

Murine macrophage-like RAW 264.7 cells were seeded into a 24-well culture plate at a density of 2×10^5 cells per well. These cells were treated for 1 h with culture

medium alone and those containing 100 μM C29 or 400 μM C29[29] and then infected with *Ab* strains (MOI = 10). For cell adhesion assay, cells were washed 3 times with PBS 30 min after infection and then lysed in 1 mL 0.2% Triton X-100. To analyze the invasion rate, DMEM medium containing 300 μg/mL gentamicin supplemented with 10% FBS was added 1 h after infection and incubated for an additional 2 h to eradicate all extracellular bacteria. In the next step, the cells were washed 3 times with PBS and lysed in 1 mL 0.2% Triton X-100 to release the invading bacteria from the infected cells. For RAW 264.7 intracellular survival assay, cells were incubated in culture medium with 300 μg/mL gentamicin for 2 h; after washing with PBS, culture medium containing 15 μg/mL gentamicin was added to control the growth of intracellular bacteria released from lysed macrophages. The cells were washed and lysed in 1 mL 0.2% Triton X-100 after an extended 4 h of incubation. The lysate was serially diluted and spread on LB agar plates.

Drug treatment *in vivo*

To test the effect of NSAIDs treatment, the mice were randomly distributed into six groups (n = 5 per group in a cage): five groups received administered intraperitoneal injections of 50 mg/kg NPXS, 100 mg/kg ASA, 10 mg/kg DXMS, 200 mg/kg AzA, and 20 mg/kg CsA 1 h before ATCC 17978 infection, and a group of ATCC 17978-infected mice received equivalent volumes of PBS. The survival rate, health status, and weight of the test animals were recorded during the next 120 h. To evaluate the therapeutic effect of NPXS treatment in immunocompromised conditions, mice received subcutaneous injection of 150 mg/kg and 100 mg/kg cyclophosphamide (MCE, Cat#HY-17420) in the first 3 days and 1 day before *Ab* infection, respectively. Subsequently, the immunocompromised mice were randomly divided into two groups (n = 5 per group in a cage): ATCC178978-infected mice with or without NPXS treatment.

Statistics

All experiments were conducted at least twice, with each experiment involving a minimum of three biological replicates. Randomized group allocation was implemented in all experiments. The sample size and the data analysis methods for each experiment is provided in the corresponding figure legends. Mean ± S.D. was utilized for data presentation unless indicated otherwise. The statistical analysis was conducted with unpaired Student's t-test between two data groups, and one-way ANOVA with Tukey correction for pairwise comparisons among three or more data groups. The Log-rank (Mantel–Cox) test was used for comparing Kaplan Meier survival curves in animal experiments. All the statistical analyses were carried out using GraphPad Prism 8 (GraphPad software). $p < 0.05$ was considered indicative of statistical significance.

Role of funders

The funders of this study had no role in study design, sample collection, data analyses, interpretation, writing of the manuscript, or the decision to publish the results.

Results

Establishing an *Ab* infection sepsis model in mice

To investigate the lethality and pathogenesis of *Ab*, a mouse sepsis infection model was established. Briefly, following i.v. infection with 7.5×10^7 CFU of ATCC strain 17978, the mortality rate of mice reached 80% at 24 h and 100% within 36 h (Fig. 1a). At 12 hpi, poor health status, decreased body weight, and splenomegaly were observed in each mouse (Fig. 1b and c). At 12 hpi, the lungs, spleen, liver, kidney and blood samples were collected from the infected mice; the bacterial load in these samples was counted and found to be as high as 10^7–10^9 CFU/g (Fig. 1d). To assess the intracellular survival of *Ab*, cells obtained from the lungs and spleen samples were incubated with 300 μg/mL gentamicin to eliminate extracellular bacteria. A significant number of ATCC 17978 was found to remain viable at 12 hpi in phagocytes; the total bacterial load was found to be higher than the intracellular population, indicating that this strain could survive in both intra- and extracellular environments (Fig. 1e), and that strain ATCC 17978 in the mouse sepsis model could not be effectively cleared by the immune system.

Ab infection-induced fluctuations in immune response and onset of cytokine storm in mice

Given the capacity of ATCC 17978 to persist intracellularly and extracellularly, we hypothesized that the symptoms of infection were induced by a hyperactive immune response triggered by the continuous stimulation of the host immune system by *Ab*. To evaluate the systemic immune response induced by *Ab*, we analyzed the changes in the number of immune cells in the lungs and spleens of *Ab*-infected mice by flow cytometry. We observed enhanced infiltration of macrophages ($CD11b^+F4/80^+$) and neutrophils ($CD11b^+Ly6G^+$), yet a decreased in the size of population of lymphocytes, including T cells ($CD19^-CD3^+$), B cells ($CD3^-CD19^+$) and natural killer (NK) cells ($CD3^-$ $NK1.1^+$) in the lungs upon *Ab* infection (Fig. 2a–d). Rapid recruitment and activation of neutrophils and macrophages were observed at the early stage of *Ab* infection. Macrophages play a crucial role in phagocytosing *Ab* and releasing cytokines that recruit neutrophils to control infection.[34] Previous studies showed that neutrophils were critical for *Ab* infection control, so that mortality rate and infection severity increased sharply in neutrophil-depleted mice.[9,35,36] In addition, lymphocytopenia is a predictor of systemic inflammatory responses caused by bacterial infection, and is characterized by reduction of T, B, and NK cells in the lungs of *Ab*-infected mice, in

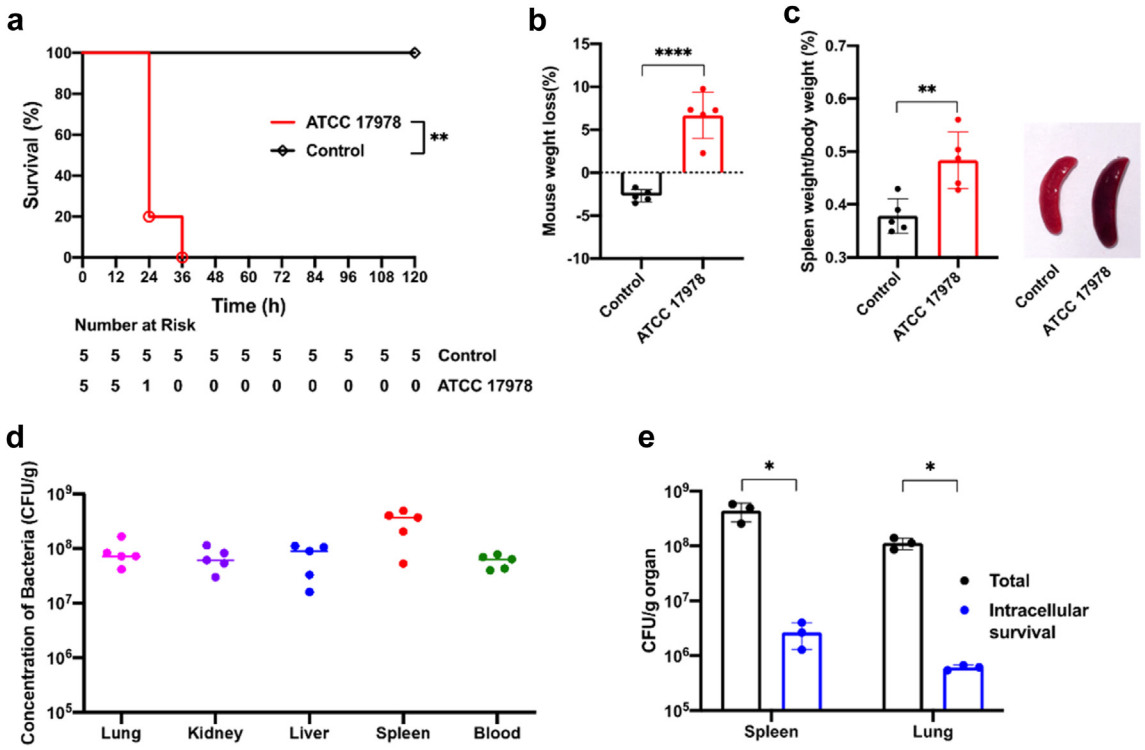

***Fig. 1:* Assessment of virulence level of *Ab* in a mouse sepsis model.** (**a**) Kaplan–Meier survival curves of mice infected by *Ab* strains (n = 5). (**b**) Relative body weight loss of *Ab*-infected mice at 12hpi (n = 5). (**c**) Percentage of spleen weight and representative image of spleens in mice after *Ab* inoculation (n = 5). (**d**) Bacteria loads in the lungs, spleen, kidney, livers and blood samples of mice at 12 hpi (n = 5). (**e**) Survival of intracellular bacteria obtained from lungs and spleen samples of the infected mice at 12 hpi (n = 5). Statistical analyses were conducted by Log-rank (Mantel–Cox) test (a) and unpaired Student's t-test (b, c, e). *$p < 0.05$, **$p < 0.01$; ***$p < 0.001$; ****$p < 0.0001$; ns, not significant.

which the CD206 MFI levels were found to decrease and the CD86 MFI levels on the surface of $CD11b^{+}F4/80^{+}$ cells increased, indicating that these cells were polarized to a pro-inflammatory M1 phenotype (Fig. 2b).

We then investigated the differences between the gene transcription levels of cells collected from healthy and infected mice using RNA-seq. It was found that a total of 3212 genes significantly up-regulated and 3514 genes were down-regulated after *Ab* infection (Supplementary Figure S2a). KEGG enrichment analysis showed that metabolic pathways that were highly responsive to infection were those involved in expression of cytokines and chemokines in innate immune system marked with red (Fig. 2e). Moreover, a relatively high expression level of the pro-inflammation (M1 polarization) markers (Fig. 2f), neutrophil activation markers (Fig. 2g), chemokines, interleukins, and TNF family (Supplementary Figure S2b–d) was depicted by constructing a heatmap. Several differentially expressed pro-inflammatory marker genes and neutrophil activation markers were selected for verification of their expression level by qRT-PCR (Fig. 2h). The levels of cytokines (TNF-α, IL-1β, and IL-6) in mouse serum were found to have increased by more than 100 folds at 12 hpi (Fig. 2i). These excessive inflammatory responses are associated with dysregulation of M1 macrophage polarization and neutrophil hyperactivation. All in all, our data suggest that *Ab* infection could systematically trigger significant macrophage polarization and neutrophil activation, lymphopenia, as well as excessive cytokine production and inflammatory response.

Revelation of functional role of macrophages in mediating excessive inflammatory response during *Ab* infection by scRNA-seq

Given the changes in the population structure of immune cells and elicitation of a strong inflammatory response during *Ab* infection, comprehensive analysis of the *Ab*-induced excessive immune response was conducted by performing scRNA-seq. Through the use of the unified single-cell analysis pipeline, a cellular landscape was generated to obtain the gene expression profile of 20,774 cells, including 11,046 from healthy mice and 9728 from ATCC 17978-infected mice. The data were presented by using the dimensionality reduction approach which involved uniform manifold approximation and projection (UMAP). Data of 14 main cell clusters are shown (Fig. 3a–c, Supplementary Figure S3a). ATCC

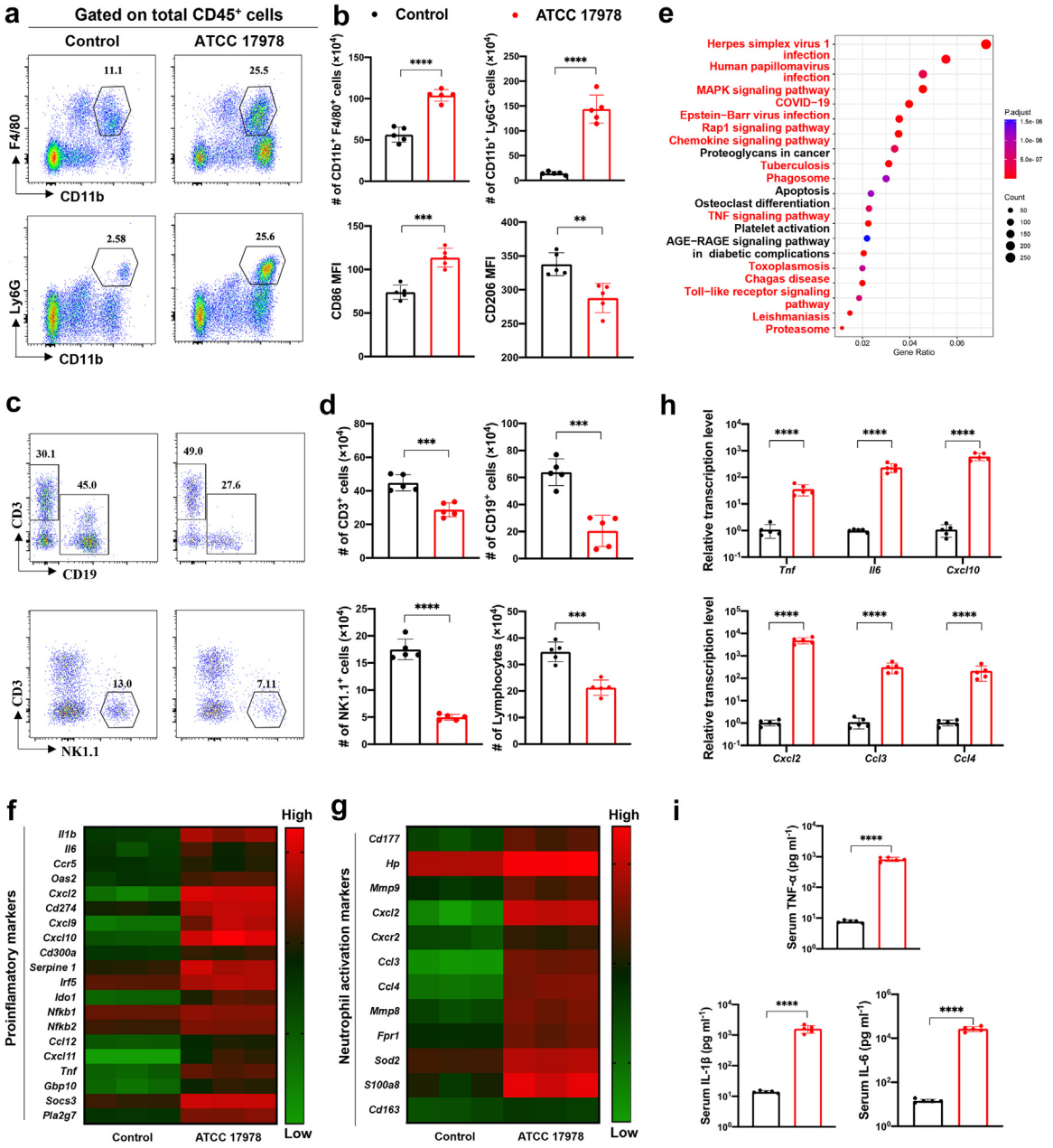

***Fig. 2: Ab*-triggered cytokine storm in the host.** (**a**) The percentages of F4/80$^+$ macrophages and Ly6G$^+$ neutrophils gated on total CD45$^+$ cells in lung cells analyzed by flow cytometry. (**b**) Quantification of total F4/80$^+$ and Ly6G$^+$ cells and expression of the surface CD86 and CD206 on F4/80$^+$ macrophages presented by mean fluorescence intensity (MFI) values in the lung cells (n = 5). (**c**) The percentages of CD3$^+$ T cells, CD19$^+$ B cells, NK1.1$^+$ NK cells gated on total CD45$^+$ cells. (**d**) Quantification of total CD3$^+$, CD19$^+$, NK1.1$^+$ cells and lymphocytes (n = 5). (**e**) KEGG enrichment analysis depicts the most affected pathways in *Ab* infection. (**f** and **g**) Heatmap which shows the differential expression patterns underlying M1 polarization (f) and neutrophil activation (g) in healthy and *Ab*-infected mice (n = 3). (**h**) The transcription levels of proinflammation (up) and chemokines (down) in different mouse groups (n = 5). (**i**) IL-1β, IL-6, TNF-α expression levels in the *Ab*-infected and non-infected mice serum (n = 5). Statistical analyses were conducted by unpaired Student's test (b, d, h, i). $^{**}p < 0.01$; $^{***}p < 0.001$; $^{****}p < 0.0001$.

17978 infection was found to result in an increase in the total number of macrophages, which was accompanied by a decrease in the frequency of detection of various lymphocyte compartments (T, B and NK cells); these findings are therefore consistent with the flow cytometry data (Fig. 3d). The lower than expected number of neutrophils could be attributed to their susceptibility to degradation, lower RNA expression level, and relatively

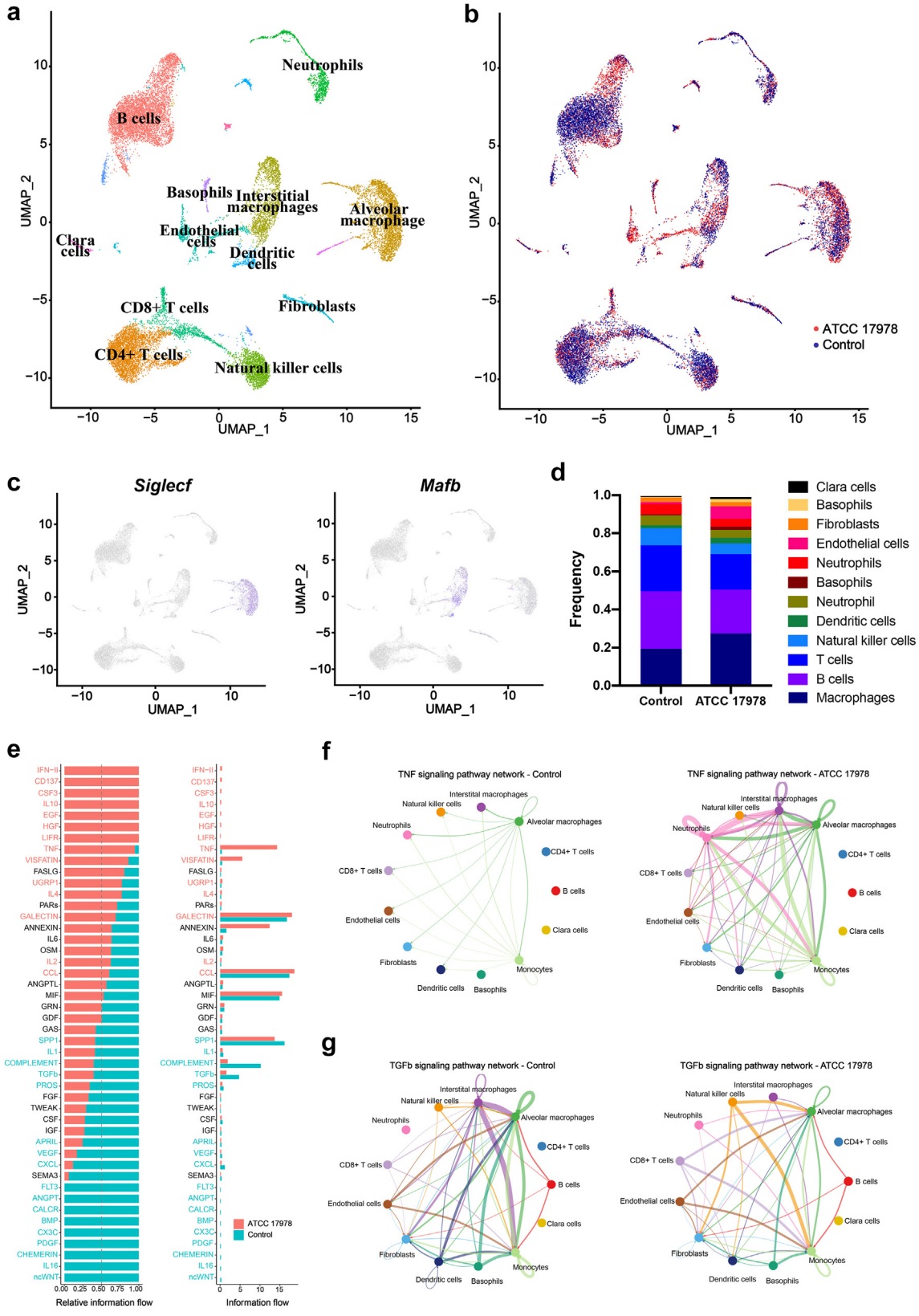
a
Neutrophils
B cells
Basophils
Interstitial macrophages
Alveolar macrophage
Endothelial cells
Clara cells
Dendritic cells
CD8+ T cells
Fibroblasts
CD4+ T cells
Natural killer cells
UMAP_1
UMAP_2
b
ATCC 17978
Control
c
Siglecf
Mafb
d
Frequency
Control
ATCC 17978
Clara cells
Basophils
Fibroblasts
Endothelial cells
Neutrophils
Basophils
Neutrophil
Dendritic cells
Natural killer cells
T cells
B cells
Macrophages
e
Relative information flow
Information flow
f
TNF signaling pathway network - Control
TNF signaling pathway network - ATCC 17978
g
TGFb signaling pathway network - Control
TGFb signaling pathway network - ATCC 17978

high levels of RNases when compared to other cells, which might result in an underestimation of the number of neutrophils in 10 × genomics scRNA-seq.[37–39] To complement the scRNA-seq data, Ly6G$^+$ neutrophils were subjected to differential expression analysis (Supplementary Figure S4a, b).

To gain further insight into the nature of interactions between different cell clusters, cell–cell communication analysis was conducted using Cellchat.[40] Global communication atlas of lung cells collected from infected and non-infected mice uncovered an overall increase in the inferred number and strength of interactions between various immune cells, as well as between immune cells and non-immune cells, upon *Ab* infection (Supplementary Figure S5a, b). The information flows of each signaling pathway were determined to depict the global immune response profiles. Upon *Ab* infection, we observed substantial enrichment of various signaling pathways, with most being associated with the inflammatory response. Intriguingly, the information flow of the signaling pathways related to pro-inflammatory response was turned on (IFN-II, CD137) or enhanced (TNF, VISFATIN), while that of the anti-proinflammatory signaling pathways decreased (TGFb) (Fig. 3e). These data indicate that inflammatory microenvironment may critically contribute to progression of *Ab*-induced sepsis. Based on this finding, we investigated the specific cellular components crucial to the relevant pathways. In the TNF signaling pathway, the total signal intensity of cell interactions in *Ab*-infected individuals was found to increase when compared to healthy individuals, especially in AMs, IMs, and neutrophils, where significantly increased signals via paracrine and autocrine was observed (Fig. 3f; Supplementary Figure S5c, e). In the TGFbeta signaling pathway, interactions of two kinds of macrophages with other immune cells were strongly attenuated, and autocrine signaling was completely lost in IMs upon *Ab* infection, whereas interactions of natural killer cells and neutrophils with other cells were enhanced (Fig. 3g, Supplementary Figure S5d, f). Neutrophils, IMs, and AMs exhibited notable changes in signal intensities in the inflammatory signaling pathway when interacting with other cells; in particular the signal intensities of IMs and AMs exhibited consistent proinflammatory trends upon *Ab* infection. Altogether, AMs and IMs were regarded as key cellular components that mediate the *Ab*-induced hyper-inflammatory response. Neutrophils also contribute to regulating the inflammatory response to *Ab* infection, although their role is less intuitive compared to that of IMs and AMs.

Ab infection induced cytokine storm in mice by modulating macrophage polarization

Given the more direct involvement of IMs and AMs in inflammatory regulation, a comprehensive investigation focused on these cell types was undertaken. Subsequently, we further performed re-clustering of these two types of macrophages and subsequently constructed the cell lineages of the differentiation trajectories to determine if M1 polarization patterns along with pseudotime could be observed upon *Ab* infection. By setting the starting point of the trajectory as CD36$^+$ M2 macrophages in AMs and Ear2$^+$ M2 macrophages in IMs, gradual evolution towards Cxcl2-labeled or Tnf-labeled M1 macrophages could be observed in both populations as pseudotime advanced. Such evolution process led to enhanced M1-like macrophages and decreased M2-like macrophages in AMs of *Ab*-infected mice when compared to healthy mice (Fig. 4a, b, c, e). The number of M1 and M2 macrophages was also found increase at a similar extent among IMs subclusters after *Ab* infection (Fig. 4f, g, h, j). The findings of pseudotime trajectory analysis therefore suggest a transition from a M2 polarization state to a M1 polarization state in IMs and AMs, and that such transition became more apparent in *Ab*-infected animals (Fig. 4c and h). This conclusion is also supported by an increase in the amount of CD86 MFI and a decrease in the amount of CD206 MFI on the surface of macrophage upon *Ab* infection, as shown in analysis by flow cytometry (Fig. 2b).

Consistently, both AMs and IMs from *Ab*-infected individuals generally exhibited enhanced expression levels of M1 polarization and proinflammatory marker genes (*Cxcl2*, *Il1b*, *Cxcl10*, *Tnf*, *Ptgs2*, *Csf3*, Fig. 4d and i, Supplementary Figure S3b, c). The enrichment analysis illustrated the vast majority of the top 20 significantly activated KEGG pathways in AMs and IMs were involved in cytokine production and robust inflammatory responses (Fig. 4k, l). Similar results were also observed in the activated KEGG pathway in Ly6G$^+$ neutrophils, involving pathways associated with

Fig. 3: **The molecular cell atlas and cell-to-cell signaling networks of lung cells depicted on the basis of single-cell RNA sequencing data.** (**a**) The UMAP projection of cells from the lungs of healthy mice and ATCC 17978-infected mice shows the main clusters and respective cell-type assignments. Each dot corresponds to an individual cell. Different colors represent different cell clusters. (**b**) Origins of cells with the same embedding as in (a). Distinct colors depict infected and non-infected lung cells. (**c**) Total RNA expression of *Siglecf* and *Mafb* in the same embedding as (a). (**d**) Frequency of detection of different types of cells shown in (a). (**e**) Differences in overall information flow in interaction networks between healthy and *Ab*-infected mice. The red-labeled signaling pathways were more enriched in infected individuals, the black-labeled signaling pathway was equally enriched in the two groups; the blue-labeled signaling pathway was more enriched in healthy individuals. **(f** and **g)** Circular plots showing the inferred intercellular communication network of the TNF signaling pathway (f) and TGFb signaling pathway (g) in healthy mice (left) and ATCC 17978-infected mice (right). The circle sizes are proportional to the number of cells in each cell group, and the edge width represents the communication probability. The edge colors correspond to the signaling source.

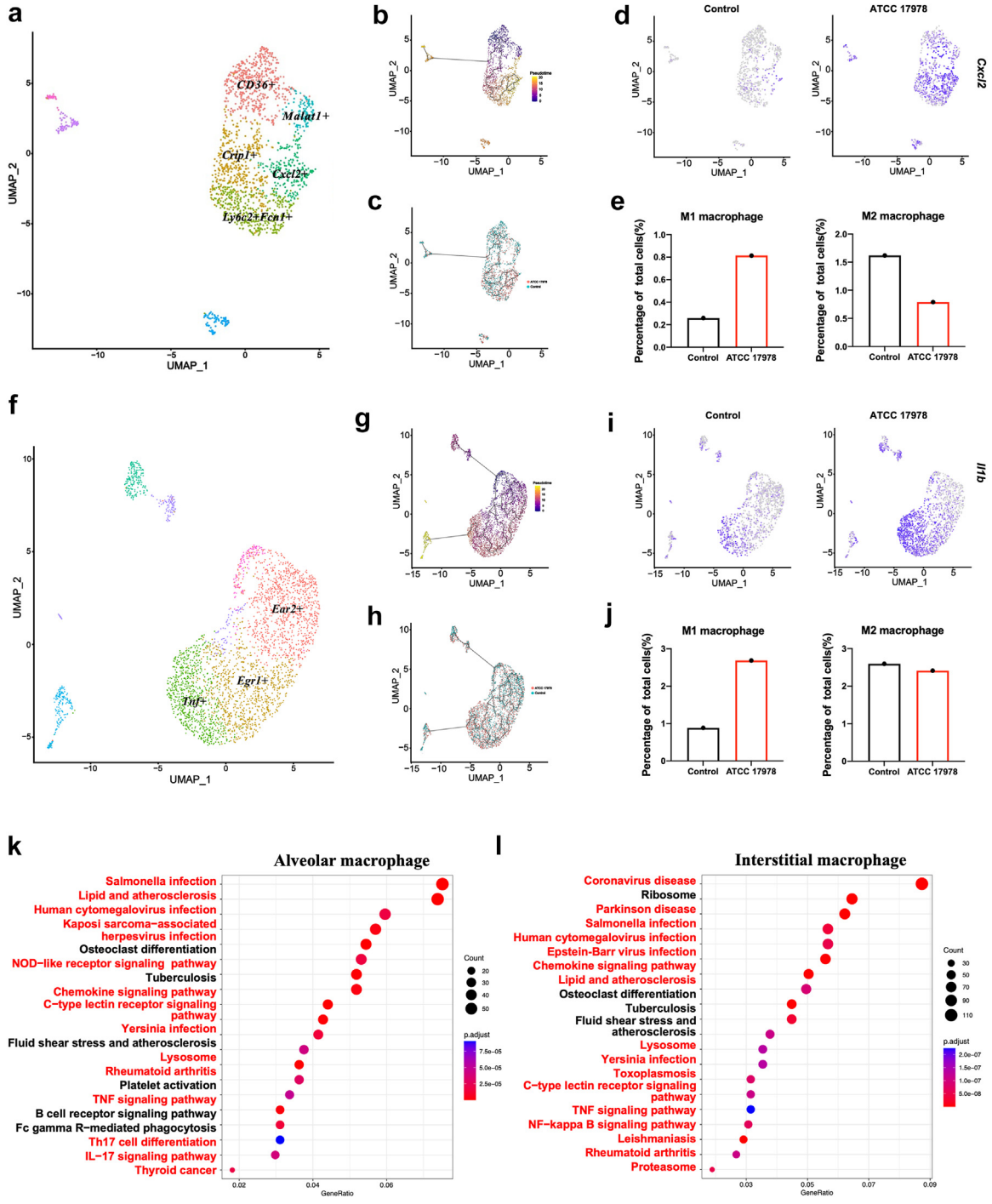

***Fig. 4: Ab* mediated onset of cytokine storm by inducing M1 polarization.** (**a**) UMAP of AMs and the corresponding group assignments. (**b** and **c**) Pseudo-time trajectory of total AM cells colored by pseudotime (b) and different samples (c). (**d**) *Cxcl2* expression of healthy and infected mice in the same embedding as (a). (**e**) Percentage of Cxcl2+ and CD36+ cells in AMs. (**f**) UMAP of IMs with cell-type assignments. (**g** and **h**) Pseudo-time trajectory of total IM cells colored by pseudotime (g) and different samples (h). (**i**) *Il1b* expression of healthy and infected mice in the same embedding as (f). (**j**) Percentage of Tnf+ and Gadd45g + cells shown in IMs. (**k** and **l**) KEGG enrichment analysis showing the most affected pathways in AMs (k) and IMs (l) upon *Ab* infection.

neurodegenerative diseases, microbial infections, and pro-inflammatory cytokines and chemokines expression, which have been reported to be potentially relevant to neutrophil chemotaxis, over-recruitment and hyperactivation (Supplementary Figure S4a).[41,42] Also, the transcript levels of most of neutrophil activation markers enhanced in the Ly6G$^+$ neutrophils of *Ab*-infected mice (Supplementary Figure S4b). Taken together, the single-cell sequencing data further confirmed that *Ab* infection promotes the polarization of IMs and AMs towards M1 phenotype and resulted in formation of cytokine storm. The findings from Ly6G$^+$ neutrophils sorting highlighted the complementary roles of neutrophil chemotaxis, over-recruitment, and hyperactivation in driving the excessive inflammatory response.

Activation of TLR2/MyD88/NF-κB signaling pathway promoted *Ab*-induced M1 macrophage polarization and elicited onset of cytokine storm

M1 polarization occurred in an inflammatory environment dominated by TLRs, which are commonly associated with activation of immune responses to combat bacterial infection.[43] Analysis of the macrophage enhancer activity revealed that NF-κB appeared to be a key transcription factor involved in M1 polarization and inflammatory response.[44] Therefore, RNA-seq and qRT-PCR were performed to analyze the differential transcription levels of TLRs commonly shared by humans and mice; the results revealed significant up-regulation of *Tlr2* expression in response to *Ab* infection. In addition, the transcript abundance of genes related to the TLR2/Myd88/NF-κB signaling pathway and expression of the downstream pro-inflammatory cytokines were also found to be increased in the lungs of *Ab*-infected mice (Fig. 5a and b). *Tlr2* was found to be highly expressed on the surface of ATCC 17978-infected macrophages when measured by flow cytometry (Fig. 5c). Furthermore, the transcriptional levels of the aforementioned genes and the pro-inflammatory marker genes were significantly enhanced, resulting in polarization of M2 macrophages toward the M1 phenotype, suggesting that expression of these genes was also elevated in IMs and AMs during *Ab* infection (Fig. 5d, Supplementary Figure S6c, d). These findings led us to hypothesize that the TLR2/Myd88/NF-κB signaling pathway was involved in the *Ab*-mediated M1 polarization, which in turn caused development of cytokine storm.

Canonical NF-κB activation primarily involves site-specific phosphorylation of the multisubunit IκB kinase (IKK) complex, triggering phosphorylation and inducible proteasome-mediated degradation of IκBα.[45,46] To demonstrate that ATCC 17978 induces NF-κB activation and translocation via TLR2/Myd88 signaling pathway, and to assess the critical role of TLR2/MyD88 in the inflammatory response, we treated *Ab*-infected RAW 264.7 with C29[29] and TJ-M2010-5.[30] Subsequently, the IKK/IκB/NF-κB expression was evaluated by Western blot, and the result showed that the total protein expression levels of IKK-α/β and NF-κB p65 remained unchanged. However, the levels of p65, IκBα, IKK-α/β phosphorylation and IκBα degradation were up-regulated in *Ab*-infected macrophages and down-regulated after treatment with C29[29] or TJ-M2010-5,[30] indicating the upregulation of TLR2 and Myd88 causes the activation of the inflammation-related IKK/IκB/NF-κB signaling pathway (Fig. 5e, Supplementary Figure S7a–d). To test the relationship between TLR2/Myd88/NF-κB signaling pathway and *Ab*-mediated cytokine storm, RAW 264.7 cells were infected with ATCC 17978 after blocking the TLR2/Myd88/NF-κB pathway with TLR2 inhibitor (C29), Myd88 inhibitor (TJ-M2010-5)[30] or NF-κB inhibitor (JSH-23).[28] We observed no difference in CD206 MFI levels, but a decrease in CD86 MFI levels when compared to cells not treated with the inhibitors (Fig. 5f and g), suggesting that the TLR2/Myd88/NF-κB pathway was involved in *Ab*-induced M1 polarization. Significant decreases were also found in IL-6 and TNF-α levels, with more than 5-fold reduction in the supernatant of RAW 264.7 observed (Fig. 5h and i). To confirm the role of TLR2 on mediating cytokine storm in *Ab* infections, TLR2 knockout (KO) and WT mice were infected with ATCC 17978. Compared to WT mice that were 100% dead at 36 hpi, *Tlr2*$^{-/-}$ mice inoculated with similar amount of *Ab* exhibited a 60% survival rate at 24 hpi and sustained a 40% survival from 36 hpi until the end of the observation, indicating a reduction of 40% in mortality compared with WT mice (Fig. 5j). In addition, we observed reduced macrophage infiltration (Fig. 5k, l), diminished M1 polarization (Fig. 5m), decreased cytokine and chemokine expression (Fig. 5n-p) in *Tlr2*$^{-/-}$ mice after *Ab* infection, indicating that the *Ab*-induced cytokine storm is TLR2-dependent. Interestingly, the living and dying populations of *Tlr2*$^{-/-}$ mice followed two different trajectories which correlated with the outcome of infection: infected mice that exhibit dramatically reduced cytokine production remain relatively healthy, yet a significant level of cytokine production was observed in morbid mice. Taken together, these findings further supported the theory that *Ab* infection could activate the TLR2/MyD88/NF-κB signaling pathway, which was a pivotal mediator of *Ab*-induced M1 macrophage polarization and hence also a strong trigger of cytokine production.

Previous studies have identified outer membrane protein A (OmpA) as a potential PAMP recognized by TLR2 in *Ab*.[47] To investigate the contribution of OmpA in onset of immune response elicited by *Ab*, we examined its effect on *Tlr2* expression and found that the transcript abundance and surface expression level of *Tlr2* was reduced in RAW264.7 infected with Δ*OmpA* (Fig. 5q, r). In the presence of C29, we observed reduced

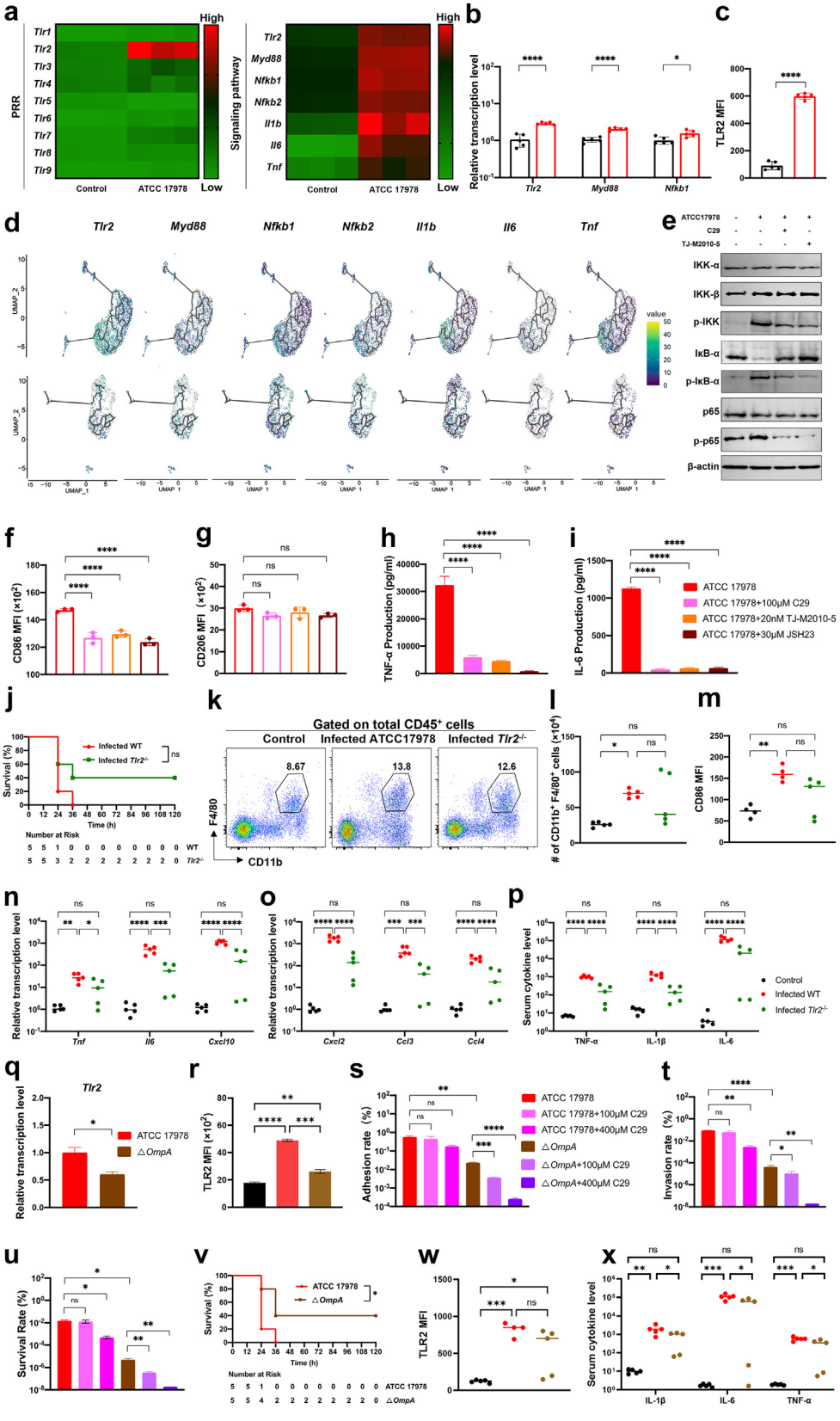
a
PRR
Tlr1
Tlr2
Tlr3
Tlr4
Tlr5
Tlr6
Tlr7
Tlr8
Tlr9
Control
ATCC 17978
High
Low
Signaling pathway
Myd88
Nfkb1
Nfkb2
Il1b
Il6
Tnf
b
Relative transcription level
c
TLR2 MFI
d
UMAP_1
UMAP_2
value
e
ATCC17978
C29
TJ-M2010-5
IKK-α
IKK-β
p-IKK
IκB-α
p-IκB-α
p65
p-p65
β-actin
f
CD86 MFI (×10²)
g
CD206 MFI (×10²)
h
TNF-α Production (pg/ml)
i
IL-6 Production (pg/ml)
ATCC 17978
ATCC 17978+100μM C29
ATCC 17978+20nM TJ-M2010-5
ATCC 17978+30μM JSH23
j
Survival (%)
Infected WT
Infected Tlr2-/-
Time (h)
Number at Risk
k
Gated on total CD45+ cells
Control
Infected ATCC17978
Infected Tlr2-/-
8.67
13.8
12.6
F4/80
CD11b
l
# of CD11b+ F4/80+ cells (×10⁴)
m
CD86 MFI
n
Relative transcription level
Tnf
Il6
Cxcl10
o
Cxcl2
Ccl3
Ccl4
p
Serum cytokine level
TNF-α
IL-1β
IL-6
Control
Infected WT
Infected Tlr2-/-
q
Tlr2
Relative transcription level
ATCC 17978
ΔOmpA
r
TLR2 MFI (×10²)
s
Adhesion rate (%)
ATCC 17978
ATCC 17978+100μM C29
ATCC 17978+400μM C29
ΔOmpA
ΔOmpA+100μM C29
ΔOmpA+400μM C29
t
Invasion rate (%)
u
Survival Rate (%)
v
Survival (%)
ATCC 17978
ΔOmpA
Time (h)
Number at Risk
w
TLR2 MFI
x
Serum cytokine level
IL-1β
IL-6
TNF-α

adhesion and invasiveness and consequently decreased survival of ATCC 17978 in macrophages. Notably, these effects were more pronounced when TLR2-inhibited macrophages were infected by the strain Δ*OmpA* (Fig. 5s-u). Consistently, compared to ATCC 17978-infected mice that were 100% dead at 36 hpi, Δ*OmpA*-infected mice exhibited a 80% survival rate at 24 hpi and maintained a 40% survival from 36 hpi onwards, indicating a dramatic reduction in mortality compared with ATCC 17978-infected mice (Fig. 5v). Moreover, lower *Tlr2* expression on the surface of macrophages and reduced cytokine levels was also found in Δ*OmpA*-infected mice (Fig. 5w and x). These observations suggest that *Ab*OmpA activated TLR2 on the surface of macrophages and induced subsequent inflammatory responses *in vivo*, indicating that OmpA may serve as one of the PAMPs of TLR2 in *Ab*-induced cytokine storm.

NPXS rescued *Ab*-infected mice by attenuating cytokine storm

To confirm that there is a high degree of correlation between onset of cytokine storm and mouse lethality upon *Ab* infection, immunosuppressive drugs were intraperitoneally administered to mice to attenuate cytokine production in infected mice and determine if mortality rate could be reduced. Another purpose of this experiment is to test whether it is feasible to develop a novel approach for treatment of *Ab* infection by suppressing the strong inflammatory response elicited by *Ab*. The therapeutic drugs utilized in this study comprised naproxen (NPXS), acetylsalicylic acid (aspirin, ASA), dexamethasone (DXMS), azathioprine (AzA), and cyclosporine A (CsA). Apart from CsA treatment, which could not improve the survival of ATCC 17978-infected mice, the administration of other immunosuppressants prolonged their survival. The survival rates of ATCC 17978-infected mice subjected to ASA, AzA, and DXMS treatment maintained 60%, 40%, and 40% from 24 hpi, 36 hpi and 48 hpi to the end of the observation, respectively, while NPXS protected 100% of the infected mice from death within 120 h, indicating its superior effectiveness compared to other treatments (Fig. 6a). Moreover, the extent of body weight loss was found to decrease from 6.7% to 3.6% and that of splenomegaly decreased from 0.48% to 0.38% on average upon NPXS treatment (Fig. 6b and c). NPXS treatment suppressed $CD11b^{+}Ly6G^{+}$ neutrophils infiltration into the lungs, while not reducing the infiltration of $CD11b^{+}F4/80^{+}$ macrophages. However, it effectively attenuated CD86 MFI levels, thereby inhibiting the macrophage polarization towards the M1 phenotype (Fig. 6d and e, Supplementary Figure S9b). Consistently, the transcript levels of most pro-inflammatory (M1 polarization) markers, neutrophil activation markers, chemokines, interleukins, TNF family (Fig. 6f and g, Supplementary Figure S10a–d) in *Ab*-infected mice were significantly lower after NPXS treatment. NPXS was also found to reduce serum cytokine production (TNF-α, IL-6 and IL-1β) in *Ab*-infected mice by more than 50-fold (Fig. 6h). These data indicated that NPXS could attenuate *Ab*-induced hyperinflammatory responses by suppressing excessive M1 macrophage polarization, neutrophil chemotaxis and hyperactivation. In addition, since *Ab* is an opportunistic bacterial pathogen that primarily infects immunocompromised individuals, we established an immunosuppressive mouse model through cyclophosphamide administration. Following treatment of these immunosuppressed mice with NPXS, the survival time of infected mice was extended, resulting in a 60% survival rate throughout the experiments (Supplementary Figure S9a). These

Fig. 5: **Blocking of the TLR2/Myd88/NF-κB pathway attenuated M1 polarization and cytokine storm caused by *Ab* infection.** (**a**) Heatmap that depicts the differential expression profile of toll-like receptor (TLR) and the TLR2/Myd88/NF-κB pathway in AMs and IMs of healthy and *Ab*-infected mice (n = 3). (**b**) The relative transcription levels of genes involved in the TLR2/Myd88/NF-κB pathway in different mice groups (n = 5). (**c**) The TLR2 MFI on the surface of $F4/80^{+}$ macrophages in the lungs of infected mice (n = 5). (**d**) Pseudo-time trajectory of total cells colored by *Tlr2*, *Myd88*, *Nfkb1*, *Nfkb2*, *Il1b*, *Il6*, *Tnf* expression levels in IMs and AMs. (**e**) Representative Western blot of cell lysis showing protein levels of total and phosphorylated IKK-α/β, IκB-α and NF-κB p65. RAW264.7 cells pretreated with culture media, C29, or TJ-M2010-5, and then infected with ATCC 17978. Beta actin was used as a loading control. (**f** and **g**) The CD86 (f) and CD206 (g) MFI on the surface of RAW264.7 cells pretreated with culture media, C29, TJ-M2010-5 or JSH-23, and then infected with ATCC 17978 (n = 3). (**h** and **i**) TNF-α (h) and IL-6 (i) levels in supernatant of *Ab*-infected RAW264.7 cells pretreated with medium, C29, TJ-M2010-5 or JSH-23 (n = 3). (**j**) Kaplan–Meier survival curves of WT and $TLR2^{-/-}$ mice infected by ATCC 17978 (n = 5). (**k**) The percentages of $F4/80^{+}$ macrophages gated on total $CD45^{+}$ cells determined by flow cytometry. (**l**) Quantification of total $F4/80^{+}$ cells analyzed in (k) (n = 5). (**m**)The surface CD86 expression on $F4/80^{+}$ macrophages in the lungs (n = 5). (**n** and **o**) The relative transcription levels of proinflammation (m) and chemokines (n) in different mice groups (n = 5). (**p**) IL-1β, IL-6, TNF-α expression levels in the healthy, infected WT and infected $Tlr2^{-/-}$ mice serum (n = 5). (**q**) mRNA expression of *Tlr2* in RAW264.7 incubated with the strains ATCC 17978 and Δ*OmpA* (MOI 5) for 3 h (n = 3). (**r**) The TLR2 MFI on the surface of RAW264.7 cells infected with ATCC 17978 and Δ*OmpA* (n = 3). (**s, t** and **u**) The adhesion rate (**s**), invasion rate (**t**) and intracellular survival efficiency (**u**) of strain ATCC 17978 and Δ*OmpA* in macrophages when treated with C29 (n = 3). (**v**) Kaplan–Meier survival curves of ATCC 17978- and Δ*OmpA-infected* mice (n = 5). (**w**) The TLR2 MFI on the surface of $F4/80^{+}$ macrophages in the lungs of healthy, ATCC 17978- and Δ*OmpA*-infected mice (n = 5). (**x**) IL-1β, IL-6, TNF-α expression levels in the healthy, ATCC 17978- and Δ*OmpA*-infected mice serum (n = 5). The Above data were analyzed using Log-rank (Mantel–Cox) test (j, v), unpaired Student's test (b, c, q) and one-way ANNOVA with Tukey's test (f-i, l-p, r-u, w, x). $^{*}p < 0.05$, $^{**}p < 0.01$; $^{***}p < 0.001$; $^{****}p < 0.0001$; ns, not significant.

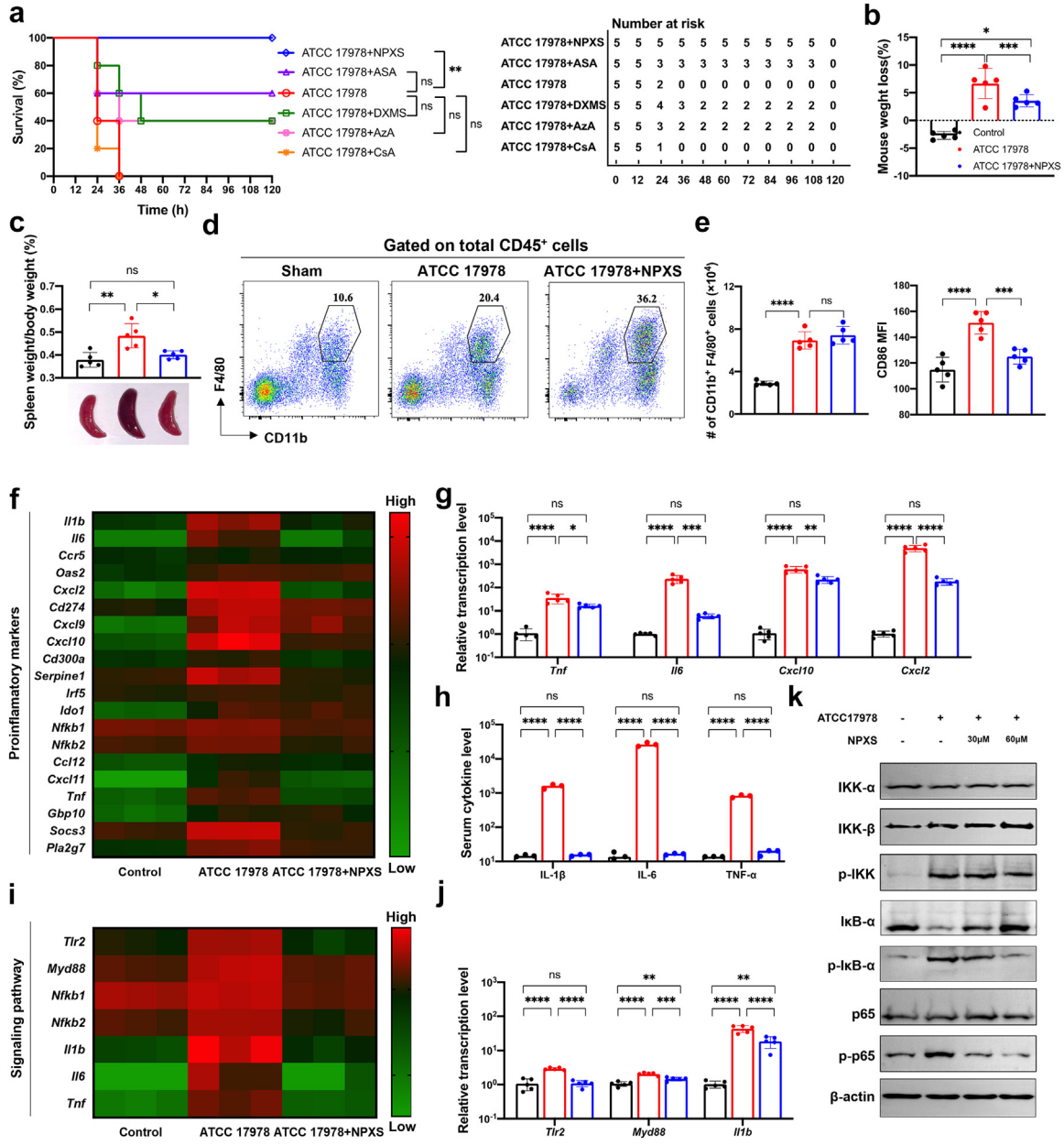

Fig. 6: **NPXS suppressed cytokine storm caused by *Ab* infection.** (**a**) Kaplan–Meier survival curves of *Ab*-infected mice treated with immunosuppressive drugs (n = 5). (**b**) Relative body weight loss of healthy, *Ab*-infected and NPXS treated *Ab*-infected mice at 12hpi (n = 5). (**c**) Percentage of spleen weight and representative image of spleens in healthy, ATCC 17978-infected, and ATCC 17978-infected + NPXS treated mice (n = 5). (**d**) The percentages of F4/80$^+$ macrophages gated on total CD45$^+$ cells determined by flow cytometry. (**e**) Quantification of total F4/80$^+$ cells analyzed in (d) and the surface CD86 expression on F4/80$^+$ macrophages in the lungs (n = 5). (**f**) Heatmap showing the differential expression profile of proinflammation marker genes in control, ATCC 17978-infected, and ATCC 17978-infected + NPXS treated mice (n = 3). (**g**) mRNA expression of M1 markers and proinflammatory cytokines in lungs of mice subjected to different treatments (n = 5). (**h**) Quantitation of IL-1β, IL-6, and TNF-α production in serum analyzed by ELISA (n = 5). (**i**) Heatmap of the TLR2/Myd88/NF-κB signaling pathway in mice of three groups (n = 3). (**j**) Relative transcription levels of the TLR2/Myd88/NF-κB signaling pathway-related genes (n = 5). (**k**) Representative Western blot of cell lysis showing protein levels of total and phosphorylated IKK-α/β, IκB-α and NF-κB p65. RAW264.7 cells pretreated with culture media, 30 μM NPXS, or 60 μM NPXS, and then infected with ATCC 17978. Beta actin was used as a loading control. Statistics were calculated by Log-rank (Mantel–Cox) test (a) and one-way ANNOVA with Tukey's test (b, c, e, g, h, j). *p < 0.05, **p < 0.01; ***p < 0.001; ****p < 0.0001; ns, not significant.

results indicated that naproxen could also provide protective effects for immunocompromised mice by attenuating the cytokine storm.

Non-steroidal anti-inflammatory drugs (NSAIDs) such as NPXS and ASA exert potent anti-inflammatory and immunosuppressive effects by inhibiting the cyclooxygenase (COX) isoforms COX-1 and COX-2.[48] Notably, both the COX-2/PGE 2 and TLR/MyD88 signaling pathways are involved in the inflammatory response, and interactions between these two different pathways are crucial for regulation of the inflammatory microenvironment.[49] RNA-seq analysis revealed that the expression levels of *Cox1* (Log_2FC:0.4194), *Cox2* (Log_2FC:0.2429) and TLR2/Myd88/NF-κB signaling pathway-related genes were suppressed in ATCC 17978-infected mice after NPXS treatment (Fig. 6i and j). Consistently, the expression levels of NF-κB p65, IκBα, IKK-α/β phosphorylation, and IκBα degradation were down-regulated after 30 μM or 60 μM naproxen treatment, which resulted in further reduction of the cytokine storm induced by *Ab* infection (Fig. 6k, Supplementary Figure S7e–h). These findings indicated that NPXS may diminish the inflammatory response by inhibiting the TLR2/Myd88/NF-κB signaling pathway in addition to COX-2/PGE2 signaling pathway. Previous studies have reported that the upregulation of the TLR/MyD88 signaling pathway could trigger NF-κB activation, which in turn induced COX-2 expression, ultimately promoting cytokine production.[44–46] Therefore, naproxen may effectively suppress COX-2 expression through the regulation of TLR2 and MyD88-mediated NF-κB activation. Taken together, these data revealed that *Ab*-induced mortality was attributed to excessive cytokine production during infection, and NPXS could serve as a novel therapeutic agent to save the lives of mice from fatal *Ab* infection by attenuating the cytokine storm.

Discussion

Ab poses a severe threat to public health. Existing approaches for treatment of *Ab* infections primarily rely totally on the use of antimicrobial agents. However, the increasing prevalence of MDR infections has made antibiotic treatments increasingly challenging. In this study, we provided a novel insight into the treatment of *Ab* infections through adopting an immunosuppressive approach. We focused on investigating the innate immune response elicited by *Ab*. In a mouse sepsis model, we found *Ab* infection led to the polarization of AMs and IMs to M1 phenotype, triggering a cytokine storm and ultimately host death. The polarization of two types of macrophages towards the M1 phenotype is primarily mediated by the TLR2/MyD88/NF-κB signaling pathway, which then triggers cytokine over-production. This excessive inflammatory response could be attenuated by NPXS, an immunosuppressant, which was found to effectively protect mice from death upon infection by *Ab*.

The immune response elicited by *Ab* is a highly complex process that involves a range of antimicrobial activities mediated by macrophages and other immune cells of the host. At the early stage of *Ab* infection, there is significant recruitment of macrophages due to activation of the innate immune response. Although the activities of macrophages are bactericidal, our findings show that a considerable number of *Ab* remained viable at 12hpi. Previous studies revealed that ATCC 17978 exhibits a higher level of virulence by evading macrophage-mediated killing.[50] This organism can therefore exhibit resistance to macrophages in the extracellular environment and deliver virulence factors into host cells, inducing apoptosis.[51] Intracellularly, *Ab* could replicate in vacuoles and escape from macrophages.[52] Several other studies also demonstrated that neutrophil extracellular traps escaping, and neutrophil-mediated phagocytosis resistance also contributed to the ability of *Ab* to resist killing by phagocytes.[53,54] The presence of viable *Ab* continuously stimulates the membrane-bound pattern recognition receptor TLR2, upregulates the TLR2/MyD88 pathway, activates the transcription factor NF-κB, and promotes M1 macrophage polarization, thereby inducing over-production of inflammatory factors (IL-1β, IL-6, and TNF-α). As a result, a severe cytokine storm is triggered, producing a systemic inflammatory response syndrome which is often associated with systemic organ failure and even death of the host.

Our findings demonstrated that the potent immune response triggered by *Ab* infection is predominantly driven by TLR2, which can recognize the PAMPs of *Ab*. PAMPs are conserved molecular motifs present in microorganisms, including lipids, proteins, carbohydrates, and nucleic acids, that enable the innate immune system to recognize pathogens.[55–57] Through binding to the LRR domain of TLRs, PAMPs induce receptor oligomerization, thereby activating them and subsequently triggering intracellular signal transduction. Some studies suggest that OmpA may be one of the PAMPs recognized by TLR2 in *Ab*.[58] *Ab*OmpA was observed to induce *Tlr2* mRNA upregulation and increase nitric oxide (NO) production in the human respiratory epithelial cell line (HEp-2).[59] Other studies have shown that *Ab*OmpA activates dendritic cells through TLR2 to induce IL-12 production, thereby stimulating $CD4^+$ T cells to respond to Th1.[60,61] Similarly, our study revealed that *Ab*OmpA increased TLR2 expression on the surface of macrophages and promoted an exaggerated inflammatory response in mice, indicating that OmpA may serve as one of the PAMPs of TLR2 in *Ab*-induced cytokine storm. However, it's important to note that OmpA is not the sole PAMP recognized by TLR2. Hence, OmpA likely plays a partial role in triggering the *Ab*-induced cytokine storm. TLR2 can also sense

bacterial lipoproteins, lipoarabinomannan, porins, peptidoglycan, lipoteichoic acid, phospholipid mannan, glycosylphosphatidylinositol anchors, glycolipids, zymosan, HSP70, hyaluronic acid, hemagglutinin, all of which have been reported to be associated with the activation of inflammatory responses.[62] Recent studies have revealed that *Ab* appears to secrete a bioactive lipid that recognizes TLR2 and activates the inflammasome signaling pathway, leading to cytokine secretion and cell death.[63] Therefore, further investigation into other PAMPs and their molecular mechanisms that contribute to the *Ab*-induced cytokine storm is needed in future studies.

The varied inflammatory responses induced by M1 macrophages exert different effects on the host innate immunity and in turn a diverse range of clinical outcomes. Moderate polarization of M1 macrophages may confer protective effects on the host during acute infectious diseases.[64] *Listeria monocytogenes* have been shown to trigger an M1 program that prevents bacterial phagosome escape and promotes intracellular bacterial killing.[65] Prolonged or excessive activation of the M1 program induces a cytokine storm, which is detrimental to the host. Uncontrolled activated M1 macrophages could produce high levels of type 1 cytokines and chemokines, which contribute to inflammation in multiple organs, with potentially fatal outcomes. Our findings first illustrated that *Ab* infection induced this uncontrolled M1 polarization and cytokine storm, which were linked to serious complications, multi-organ failure and death of the host. Cytokine storm is also known to be triggered by various viruses, bacteria, or fungi infections. Several Gram-negative bacteria have been reported to cause the excessive inflammatory response in the host, these include *Yersinia pestis*,[10] *Francisella tularensis*,[66] *Pseudomonas aeruginosa*,[67] and *Klebsiella pneumoniae*.[42] Hence, inhibiting hyperpolarization of M1 macrophages or excessive expression of cytokines may represent a novel approach for the treatment of infections caused by *Ab* and other pathogens, regardless of their antibiotic susceptibility profiles. Additionally, certain pathogen infections, such as COVID-19 and *Klebsiella pneumoniae*, may trigger excessive neutrophil infiltration and abnormal activation.[42,68] The substantial release of cytokines and chemokines during severe pathogen infection significantly enhances neutrophil recruitment, activation, and chemotaxis.[69,70]

In our study, the immunosuppressive drugs could be used to suppress the inflammatory response induced during *Ab* infection. Our results showed that NSAIDs (ASA and NPXS) exhibited relatively high efficacy as a therapeutic agent that acts by inhibiting the *Ab*-triggered cytokine storm, with naproxen being the most effective. Naproxen attenuated the excessive *Ab*-induced inflammatory response by inhibiting the M1 macrophage polarization and neutrophil activation. A previous study also demonstrated the effectiveness of naproxen to control the cytokine storm in chronic and severe cases of COVID-19 diseases.[71] Naproxen, a nonselective inhibitor of COX-1 and COX-2, suppresses the constitutive expression of COX-1 in most cells, as well as the induced expression of COX-2 in response to inflammatory stimuli.[72] In this study, we found that the anti-inflammatory potency of aspirin recorded during *Ab* infection was inferior to that of naproxen. COX-2 has been regarded as the most suitable target for anti-inflammatory drugs. Also, it was shown that the therapeutic anti-inflammatory effect of NSAIDs is achieved by inhibiting COX-2, whereas the adverse side effects are primarily associated with COX-1 inhibition.[73] The superior inhibitory effect of naproxen on COX-2 compared to aspirin results in evidence of disparity in the anti-inflammatory effects and potency of the two drugs. In addition, the effect of naproxen is more long-lasting and fewer doses are required for treatment.

Our study has some limitations. On one hand, although interstitial and alveolar macrophages act as main targets in the cytokine storm induced by *Ab* infection, other immune populations involved in this process, such as T cells, B cells, and natural killer cells, still need to be further explored. On the other hand, our study indicates that OmpA may act as a PAMP recognized by TLR2 in *Ab*-induced cytokine storm. However, *Ab*OmpA may not be the sole PAMP recognized by TLR2, and further research is necessary to explore additional PAMPs and their molecular mechanisms contributing to *Ab*-induced cytokine storm.

In summary, this study reveals the intricate immune response triggered by *Ab* infections, revealing a critical link between macrophage polarization, neutrophil activation, cytokine storm, and host mortality. The findings highlighted the pivotal role of the TLR2/MyD88/NF-κB signaling pathway in driving the excessive inflammatory response. Importantly, given that anti-inflammatory drugs such as naproxen can effectively protect mice from potentially fatal *Ab* infection, this drug can be considered as a promising therapeutic agent for treatment of human infections in the future.

Contributors

HW performed the investigations and drafted the manuscript; HW and QX designed the project; QX and MXP helped with animal experiments; HH analyzed the scRNA- and RNA-sequencing data; QX, WXZ, YT, BKC, KCC, HYHN, and MMX provided technical support in various experiments; QX and EWC edited the manuscript; GY and SC supervised the project and wrote the manuscript. HW and SC have directly accessed and verified the underlying data reported in the manuscript. All authors read and approved the final manuscript for publication.

Data sharing statement

The raw RNA-seq data from whole mouse lung and Ly6G$^+$ cells have been deposited in NCBI database with the accession numbers PRJNA1019086 and PRJNA1098436, respectively. Raw scRNA-seq sequencing reads are available in the NCBI database with the accession number PRJNA1099127. All other data are available in the main text or the Supplementary Materials.

Declaration of interests
Authors declare that they have no competing interests.

Acknowledgements
This work described in this paper was supported by grants provided by the Research Grants Council of the Hong Kong Special Administrative Region, China (Project Reference Number: T11-104/22-R and R1011-23).

Appendix A. Supplementary data
Supplementary data related to this article can be found at https://doi.org/10.1016/j.ebiom.2024.105340.

References

1 Giammanco A, Calà C, Fasciana T, Dowzicky MJ. Global assessment of the activity of tigecycline against multidrug-resistant Gram-negative pathogens between 2004 and 2014 as part of the tigecycline evaluation and surveillance trial. *mSphere*. 2017;2(1):e00310-16.
2 Rolain J-M, Diene SM, Kempf M, Gimenez G, Robert C, Raoult D. Real-time sequencing to decipher the molecular mechanism of resistance of a clinical pan-drug-resistant Acinetobacter baumannii isolate from Marseille, France. *Antimicrob Agents Chemother*. 2013;57(1):592–596.
3 Ayoub Moubareck C, Hammoudi Halat D. Insights into Acinetobacter baumannii: a review of microbiological, virulence, and resistance traits in a threatening nosocomial pathogen. *Antibiotics*. 2020;9(3):119.
4 Morris FC, Dexter C, Kostoulias X, Uddin MI, Peleg AY. The mechanisms of disease caused by Acinetobacter baumannii. *Front Microbiol*. 2019;10:1601.
5 But A, Yetkin MA, Kanyilmaz D, et al. Analysis of epidemiology and risk factors for mortality in ventilator-associated pneumonia attacks in intensive care unit patients. *Turk J Med Sci*. 2017;47(3):812–816.
6 Dickstein Y, Lellouche J, Ben Dalak Amar M, et al. Treatment outcomes of colistin-and carbapenem-resistant Acinetobacter baumannii infections: an exploratory subgroup analysis of a randomized clinical trial. *Clin Infect Dis*. 2019;69(5):769–776.
7 García-Patiño MG, García-Contreras R, Licona-Limón P. The immune response against Acinetobacter baumannii, an emerging pathogen in nosocomial infections. *Front Immunol*. 2017;8:441.
8 Wong D, Nielsen TB, Bonomo RA, Pantapalangkoor P, Luna B, Spellberg B. Clinical and pathophysiological overview of Acinetobacter infections: a century of challenges. *Clin Microbiol Rev*. 2017;30(1):409–447.
9 Qiu H, KuoLee R, Harris G, Van Rooijen N, Patel GB, Chen W. Role of macrophages in early host resistance to respiratory Acinetobacter baumannii infection. *PLoS One*. 2012;7(6):e40019.
10 Fajgenbaum DC. June CH. Cytokine storm. *N Engl J Med*. 2020;383(23):2255–2273.
11 Sameer AS, Nissar S. Toll-like receptors (TLRs): structure, functions, signaling, and role of their polymorphisms in colorectal cancer susceptibility. *BioMed Res Int*. 2021;2021.
12 Chen W. Host innate immune responses to Acinetobacter baumannii infection. *Front Cell Infect Microbiol*. 2020;10:486.
13 Knapp S, Wieland CW, Florquin S, et al. Differential roles of CD14 and toll-like receptors 4 and 2 in murine Acinetobacter pneumonia. *Am J Respir Crit Care Med*. 2006;173(1):122–129.
14 Kim CH, Kim DJ, Lee SJ, et al. Toll-like receptor 2 promotes bacterial clearance during the initial stage of pulmonary infection with Acinetobacter baumannii. *Mol Med Rep*. 2014;9(4):1410–1414.
15 Kim C-H, Jeong Y-J, Lee J, et al. Essential role of toll-like receptor 4 in Acinetobacter baumannii-induced immune responses in immune cells. *Microb Pathog*. 2013;54:20–25.
16 Mukherjee S, Karmakar S, Babu SPS. TLR2 and TLR4 mediated host immune responses in major infectious diseases: a review. *Braz J Infect Dis*. 2016;20:193–204.
17 March C, Regueiro V, Llobet E, et al. Dissection of host cell signal transduction during Acinetobacter baumannii–triggered inflammatory response. *PLoS One*. 2010;5(4):e10033.
18 Park M-K, Park H-K, Yu HS. Toll-like receptor 2 mediates Acanthamoeba-induced allergic airway inflammatory response in mice. *PLoS Neglected Trop Dis*. 2023;17(1):e0011085.
19 Zhai Y, Ao L, Yao Q, The E, Fullerton DA, Meng X. Elevated expression of TLR2 in aging hearts exacerbates cardiac inflammatory response and adverse remodeling following ischemia and reperfusion injury. *Front Immunol*. 2022;13:891570.
20 Nakao M, Sugaya M, Fujita H, et al. TLR2 deficiency exacerbates imiquimod-induced psoriasis-like skin inflammation through decrease in regulatory T cells and impaired IL-10 production. *Int J Mol Sci*. 2020;21(22):8560.
21 Lin K, Luo W, Yan J, et al. TLR2 regulates angiotensin II-induced vascular remodeling and EndMT through NF-κB signaling. *Aging (Albany NY)*. 2021;13(2):2553.
22 Yang G, Song W, Xu J, et al. Pik3c3 deficiency in myeloid cells imparts partial resistance to experimental autoimmune encephalomyelitis associated with reduced IL-1β production. *Cell Mol Immunol*. 2021;18(8):2024–2039.
23 Kim D, Langmead B, Salzberg SL. HISAT: a fast spliced aligner with low memory requirements. *Nat Methods*. 2015;12(4):357–360.
24 Liao Y, Smyth GK, Shi W. featureCounts: an efficient general purpose program for assigning sequence reads to genomic features. *Bioinformatics*. 2014;30(7):923–930.
25 Love M, Huber W, Anders S. Moderated estimation of fold change and dispersion for RNA-seq data with DESeq2 Genome Biology. 2014;15(12):550.
26 Stuart T, Butler A, Hoffman P, et al. Comprehensive integration of single-cell data. *Cell*. 2019;177(7):1888–1902.e21.
27 Cao J, Spielmann M, Qiu X, et al. The single-cell transcriptional landscape of mammalian organogenesis. *Nature*. 2019;566(7745):496–502.
28 Shin H-M, Kim M-H, Kim BH, et al. Inhibitory action of novel aromatic diamine compound on lipopolysaccharide-induced nuclear translocation of NF-κB without affecting IκB degradation. *FEBS Lett*. 2004;571(1–3):50–54.
29 Mistry P, Laird MH, Schwarz RS, et al. Inhibition of TLR2 signaling by small molecule inhibitors targeting a pocket within the TLR2 TIR domain. *Proc Natl Acad Sci USA*. 2015;112(17):5455–5460.
30 Xie L, Jiang F-C, Zhang L-M, et al. Targeting of MyD88 homodimerization by novel synthetic inhibitor TJ-M2010-5 in preventing colitis-associated colorectal cancer. *J Natl Cancer Inst*. 2016;108(4).
31 Wang Y, Wang ZP, Chen Y, Hua XT, Yu YS, Ji QJ. A highly efficient CRISPR-Cas9-based genome engineering platform in acinetobacter baumannii to understand the H2O2-sensing mechanism of OxyR. *Cell Chem Biol*. 2019;26(12):1732-+.
32 Wang Y, Wang Z, Ji Q. CRISPR-Cas9-Based genome editing and cytidine base editing in acinetobacter baumannii. *STAR Protoc*. 2020;1(1):100025.
33 Xie S, Shen B, Zhang C, Huang X, Zhang Y. sgRNAcas9: a software package for designing CRISPR sgRNA and evaluating potential off-target cleavage sites. *PLoS One*. 2014;9(6):e100448.
34 Liu Z, Xu W. Neutrophil and macrophage response in acinetobacter baumannii infection and their relationship to lung injury. *Front Cell Infect Microbiol*. 2022;12:890511.
35 Van Faassen H, KuoLee R, Harris G, Zhao X, Conlan JW, Chen W. Neutrophils play an important role in host resistance to respiratory infection with Acinetobacter baumannii in mice. *Infect Immun*. 2007;75(12):5597–5608.
36 Bhuiyan MS, Ellett F, Murray GL, et al. Acinetobacter baumannii phenylacetic acid metabolism influences infection outcome through a direct effect on neutrophil chemotaxis. *Proc Natl Acad Sci USA*. 2016;113(34):9599–9604.
37 Single-cell RNA-seq methods to interrogate virus-host interactions. In: Ratnasiri K, Wilk AJ, Lee MJ, Khatri P, Blish CA, eds. *Seminars in immunopathology*. Springer; 2023.
38 Ekpenyong AE, Toepfner N, Chilvers ER, Guck J. Mechanotransduction in neutrophil activation and deactivation. *Biochim Biophys Acta Mol Cell Res*. 2015;1853(11):3105–3116.
39 Yap B, Kamm RD. Mechanical deformation of neutrophils into narrow channels induces pseudopod projection and changes in biomechanical properties. *J Appl Physiol*. 2005;98(5):1930–1939.
40 Jin S, Guerrero-Juarez CF, Zhang L, et al. Inference and analysis of cell-cell communication using CellChat. *Nat Commun*. 2021;12(1):1088.
41 Chakraborty S, Tabrizi Z, Bhatt NN, Franciosa SA, Bracko O. A brief overview of neutrophils in neurological diseases. *Biomolecules*. 2023;13(5):743.
42 Xu Q, Xie M, Liu X, et al. Molecular mechanisms underlying the high mortality of hypervirulent Klebsiella pneumoniae and its

effective therapy development. *Signal Transduct Targeted Ther*. 2023;8(1):221.
43 Murray PJ. Macrophage polarization. *Annu Rev Physiol*. 2017;79:541–566.
44 Tugal D, Liao X, Jain MK. Transcriptional control of macrophage polarization. *Arterioscler Thromb Vasc Biol*. 2013;33(6):1135–1144.
45 Karin M, Yamamoto Y, Wang QM. The IKK NF-κB system: a treasure trove for drug development. *Nat Rev Drug Discov*. 2004;3(1):17–26.
46 Kim HJ, Hawke N, Baldwin AS. NF-κB and IKK as therapeutic targets in cancer. *Cell Death Differ*. 2006;13(5):738–747.
47 Schweppe DK, Harding C, Chavez JD, et al. Host-microbe protein interactions during bacterial infection. *Chem Biol*. 2015;22(11):1521–1530.
48 Wongrakpanich S, Wongrakpanich A, Melhado K, Rangaswami J. A comprehensive review of non-steroidal anti-inflammatory drug use in the elderly. *Aging Dis*. 2018;9(1):143.
49 Echizen K, Hirose O, Maeda Y, Oshima M. Inflammation in gastric cancer: interplay of the COX-2/prostaglandin E2 and Toll-like receptor/MyD88 pathways. *Cancer Sci*. 2016;107(4):391–397.
50 Lin L, Tan B, Pantapalangkoor P, et al. Inhibition of LpxC protects mice from resistant Acinetobacter baumannii by modulating inflammation and enhancing phagocytosis. *mBio*. 2012;3(5):e00312-12.
51 Jin JS, Kwon S-O, Moon DC, et al. Acinetobacter baumannii secretes cytotoxic outer membrane protein A via outer membrane vesicles. *PLoS One*. 2011;6(2):e17027.
52 Sycz G, Di Venanzio G, Distel JS, et al. Modern Acinetobacter baumannii clinical isolates replicate inside spacious vacuoles and egress from macrophages. *PLoS Pathog*. 2021;17(8):e1009802.
53 Ríos-López AL, González G, Hernández-Bello R, Sánchez-González A. Avoiding the trap: mechanisms developed by pathogens to escape neutrophil extracellular traps. *Microbiol Res*. 2021;243:126644.
54 Baz AA, Hao H, Chen S, Chu Y. Neutrophil extracellular traps in bacterial infections and evasion strategies. *Front Immunol*. 2024;15:1357967.
55 Tang D, Kang R, Coyne CB, Zeh HJ, Lotze MT. PAMP s and DAMP s: signal 0s that spur autophagy and immunity. *Immunol Rev*. 2012;249(1):158–175.
56 Levinson W. *Review of medical microbiology and immunology*. McGraw-Hill Education; 2014.
57 Silva-Gomes S, Decout A, Nigou J. *Pathogen-associated molecular patterns (PAMPs)*. Encyclopedia of Inflammatory Diseases; 2015:1–16.
58 Mogensen TH. Pathogen recognition and inflammatory signaling in innate immune defenses. *Clin Microbiol Rev*. 2009;22(2):240–273.
59 Kim SA, Yoo SM, Hyun SH, et al. Global gene expression patterns and induction of innate immune response in human laryngeal epithelial cells in response to Acinetobacter baumannii outer membrane protein A. *FEMS Immunol Med Microbiol*. 2008;54(1):45–52.
60 Li F-J, Starrs L, Burgio G. Tug of war between Acinetobacter baumannii and host immune responses. *Pathog Dis*. 2018;76(9):ftz004.
61 Lee JS, Lee JC, Lee C-M, et al. Outer membrane protein A of Acinetobacter baumannii induces differentiation of CD4+ T cells toward a Th1 polarizing phenotype through the activation of dendritic cells. *Biochem Pharmacol*. 2007;74(1):86–97.
62 Vidya MK, Kumar VG, Sejian V, Bagath M, Krishnan G, Bhatta R. Toll-like receptors: significance, ligands, signaling pathways, and functions in mammals. *Int Rev Immunol*. 2018;37(1):20–36.
63 Tiku V, Kew C, Kofoed EM, Peng Y, Dikic I, Tan M-W. Acinetobacter baumannii secretes a bioactive lipid that triggers inflammatory signaling and cell death. *Front Microbiol*. 2022:1327.
64 Shaughnessy LM, Swanson JA. The role of the activated macrophage in clearing Listeria monocytogenes infection. *Front Biosci*. 2007;12:2683.
65 Pfeffer K, Matsuyama T, Kündig TM, et al. Mice deficient for the 55 kd tumor necrosis factor receptor are resistant to endotoxic shock, yet succumb to L. monocytogenes infection. *Cell*. 1993;73(3):457–467.
66 D'Elia RV, Harrison K, Oyston PC, Lukaszewski RA, Clark GC. Targeting the "cytokine storm" for therapeutic benefit. *Clin Vaccine Immunol*. 2013;20(3):319–327.
67 Tisoncik JR, Korth MJ, Simmons CP, Farrar J, Martin TR, Katze MG. Into the eye of the cytokine storm. *Microbiol Mol Biol Rev*. 2012;76(1):16–32.
68 Lang FM, Lee KM-C, Teijaro JR, Becher B, Hamilton JA. GM-CSF-based treatments in COVID-19: reconciling opposing therapeutic approaches. *Nat Rev Immunol*. 2020;20(8):507–514.
69 Hu B, Huang S, Yin L. The cytokine storm and COVID-19. *J Med Virol*. 2021;93(1):250–256.
70 Ma Y, Zhang Y, Zhu L. Role of neutrophils in acute viral infection. *Immun Inflamm Dis*. 2021;9(4):1186–1196.
71 Dayer MR. Analgesics candidates for JAK-STAT pathway inhibition as a probable treat for COVID-19, bioinformatics study. *Biomacromolecular J*. 2021;7(1):10–17.
72 Valentovic M. *xPharm: the comprehensive pharmacology reference*. Elsevier; 2007.
73 Zarghi A, Arfaei S. Selective COX-2 inhibitors: a review of their structure-activity relationships. *Iran J Pharm Res*. 2011;10(4):655.